d-wave superconductivity and Bogoliubov-Fermi surfaces in Rarita-Schwinger-Weyl semimetals

Julia M. Link [1,*] Igor Boettcher,[2,†] and Igor F. Herbut [1,‡]

[1]*Department of Physics, Simon Fraser University, Burnaby, British Columbia, Canada V5A 1S6*
[2]*Joint Quantum Institute, University of Maryland, College Park, Maryland 20742, USA*

We uncover the properties of complex tensor (*d*-wave) superconducting order in three-dimensional Rarita-Schwinger-Weyl semimetals that host pseudospin-$\frac{3}{2}$ fermions at a fourfold linear band-crossing point. Although the general theory of *d*-wave order was originally developed for materials displaying quadratic band touching, it directly applies to the case of semimetals with linear dispersion, several candidate compounds of which have been discovered experimentally very recently. The spin-$\frac{3}{2}$ nature of the fermions allows for the formation of spin-2 Cooper pairs which may be described by a complex second-rank tensor order parameter. In the case of linear dispersion, for the chemical potential at the Fermi point and at strong coupling, the energetically preferred superconducting state is the uniaxial nematic state, which preserves time-reversal symmetry and provides a full (anisotropic) gap for quasiparticle excitations. In contrast, at a finite chemical potential, we find that the usual weak-coupling instability is toward the "cyclic state," well known from the studies of multicomponent Bose-Einstein condensates, which breaks time-reversal symmetry maximally, has vanishing average value of angular momentum, and features 16 small Bogoliubov-Fermi surfaces. The Rarita-Schwinger-Weyl semimetals provide therefore the first example of weakly coupled, three-dimensional, isotropic *d*-wave superconductors where the *d*-wave superconducting phase is uniquely selected by the quartic expansion of the mean-field free energy, and is not afflicted by the accidental degeneracy first noticed by Mermin over 40 years ago. We discuss the appearance and stability of the Bogoliubov-Fermi surfaces in absence of inversion symmetry in the electronic Hamiltonian, as in the case at hand.

The observation of exotic fermions with higher effective spin as low-energy degrees of freedom in many novel materials paves the way toward exploring quantum many-body phases at the interface of condensed-matter physics and high-energy physics. Over the last years, semimetals with Fermi points that host Dirac particles [1], Weyl fermions [2,3], or fermions at a quadratic band-touching point [4–8] have been investigated intensively. Very recent ground-breaking experiments have observed higher-spin fermions with large topological charge and associated long Fermi arcs in surface states [9–17]. Among the candidates for an explanation of the measurements, in PdBiSe [16] for instance, is the famous Rarita-Schwinger-Weyl (RSW) fermion with linear energy-momentum relation and the effective spin of $\frac{3}{2}$ [18–21]. Although in its original Lorentz-invariant [Rarita-Schwinger (RS)] version it may be allowed to appear as an elementary particle, the RS fermion is not part of the current standard model of particle physics, although it appears in its supergravity extensions [22]. This leaves the solid state as presently the only platform to study its fundamental properties and interactions.

The physics of spin-$\frac{3}{2}$ particles in electronic systems is potentially very rich. Here we focus on three-dimensional materials, where the time-reversal-invariant, inversion-symmetry-odd, helicity operator $h = \mathbf{p} \cdot \mathbf{J}$ is well defined, with momentum $\mathbf{p} = (p_x, p_y, p_z)$ and 4×4 spin-$\frac{3}{2}$ matrices $\mathbf{J} = (J_x, J_y, J_z)$. For any low-energy $k \cdot p$ Hamiltonian H constructed from h, helicity is a good quantum number, and so it is meaningful to associate an effective "spin" to the corresponding fermion. The two simplest cases are comprised by the RSW Hamiltonian $H = \mathbf{p} \cdot \mathbf{J}$, describing a rotationally invariant linear four-band crossing, and the celebrated Luttinger Hamiltonian $H = (\mathbf{p} \cdot \mathbf{J})^2 - \frac{5}{4} p^2$, describing a fourfold quadratic band touching [23–25]. In either case, the fermion near the Fermi point is described by a four-component spinor or, equivalently, by four distinct fermion operators. The interaction terms that can be constructed from these could lead to several possible exotic broken-symmetry phases, including nematic order [26–29], unconventional superconductivity [30–48], or tensorial magnetism [49–57]. Consequently, semimetals featuring higher-spin fermions provide a natural platform for observing novel quantum states of matter. First studies of the effects of electron-electron interactions in RSW and RSW-type semimetals appeared in Refs. [21,58,59].

A hallmark of superconductivity in multiband systems such as those featuring spin-$\frac{3}{2}$ fermionic quasiparticles is the possibility to form Cooper pairs with an effective spin higher than unity. The superconducting order parameter, for example, can be a five-component condensate of spin 2, which is a three-dimensional spatially homogeneous "*d*-wave" state.

*jmlink@sfu.ca
†iboettch@umd.edu
‡iherbut@sfu.ca

One can also think of the same d-wave order parameter as a complex second-rank irreducible tensor [40]. In this mathematically equivalent representation it becomes a complex symmetric traceless matrix ϕ which transforms as $\phi \to R\phi R^T$ under rotations $R \in \mathrm{SO}(3)$. If ϕ is real, up to a possible overall phase common to all components, the corresponding superconducting state preserves time-reversal symmetry, and obviously $\mathrm{tr}(\phi^*\phi) = \mathrm{tr}(\phi^2)$. In contrast, genuinely complex (again, meaning apart from an overall phase) matrices ϕ break time-reversal symmetry, and $\mathrm{tr}(\phi^*\phi) > |\mathrm{tr}(\phi^2)|$. In particular, if $\phi \neq 0$ but $\mathrm{tr}(\phi^2) = 0$, we would say that the time-reversal symmetry in the d-wave superconducting state is broken *maximally*.

The phase diagram of complex tensor order in Luttinger semimetals with a quadratic band-touching point has been investigated in Refs. [40,43,45,60]. For the chemical potential at the Fermi point ($\mu = 0$ in the following), there is a phase transition at strong coupling into a real uniaxial nematic phase. The uniaxial state, with two parallel circles of line nodes, is selected among the real order parameters, that are left degenerate by the quartic terms, by the sextic terms in the Ginzburg-Landau free energy. For $\mu > 0$, on the other hand, there is a weak-coupling second-order phase transition into a phase that breaks time-reversal symmetry. Surprisingly, just as at $\mu = 0$, an expansion of the mean-field free energy to quartic order does not suffice to determine the energetically optimal ordered configuration [61]. At the level of mean-field theory, one can either employ the sextic term [40] in the expansion, or determine the ground state of the full mean-field BCS free energy at zero temperature exactly [60], with qualitatively the same, and even quantitatively very close, outcomes. In particular, the latter approach yields a C_{2z}-symmetric superconducting ground state that breaks time-reversal symmetry almost maximally, with a high magnetization, which overlaps with the state obtained by minimization of the sextic term better than 99%. The so-called cyclic state, which breaks time-reversal symmetry maximally, but in spite of that shows vanishing average magnetization, turns out to be only a local, but not the global minimum of the mean-field Ginzburg-Landau free energy at weak coupling. Thermal and quantum fluctuations have also been studied in Ref. [43]. In particular, it was shown that their effect is to *generate* the quartic term missing in the weak-coupling derivation of the Ginzburg-Landau free energy, and with the sign that favors the formation of the cyclic state right below the critical temperature.

In this work, we study the complex tensor (spin 2) order in superconducting RSW semimetals within the mean-field approximation, and assuming a local (momentum-independent) pairing interaction. A possibility of unconventional superconductivity also arises in other semimetals [62–64]. Despite the modified band structure, the overall phase diagram resembles that of the Luttinger semimetals, but with several important novel features. For strong coupling and $\mu = 0$, the superconducting state is symmetric under time reversal and again the uniaxial nematic state is selected among the real order parameters by the sextic terms in the Ginzburg-Landau free energy. In the RSW semimetals, however, the uniaxial nematic state opens a full gap for $\mu = 0$. At weak coupling and $\mu > 0$, the ground state again breaks the time-reversal symmetry. Most importantly, and in contrast to the case of

parabolic dispersion, the expansion of the mean-field free energy to quartic order in the order parameter now suffices to fully determine the cyclic state as the optimal superconducting ground state right below the critical temperature. We compare d-wave orders in Luttinger and RSW semimetals in Table I. Experimental signatures of complex tensor order would appear, for instance, in the angular or energy dependence of the optical conductivity [65–69], and in magnetic properties. Another distinguishing feature of multiband superconductors is the potential formation of Bogoliubov-Fermi (BF) surfaces in time-reversal symmetry-breaking superconducting states, i.e., codimension-1 surfaces of gapless quasiparticle excitations [36,70–74]. Potential experimental signatures of BF surfaces have recently been discussed in Ref. [75]. As first laid out in Ref. [36], such surfaces are topologically protected in inversion-symmetric systems. They may, however, be inherently unstable toward spontaneous breaking of inversion symmetry, in presence of a favorable interaction [76]. Clearly, the single-particle Hamiltonian in RSW semimetals breaks inversion symmetry, which makes it immune to the afore-mentioned instability, but at the same time the appearance and the concomitant stability of the BF surfaces we find in all time-reversal-breaking superconducting states we checked might not be generic. Nevertheless, we report that the superconducting cyclic state which arises in RSW weakly coupled semimetals features 16 small BF surfaces, which are nondegenerate at each value of the momentum, and hence are automatically stable in presence of weak perturbations. The properties of superconductors breaking both inversion and time-reversal symmetries recently came into focus due to applications in two-dimensional structures such as monolayer transition metal dichalcogenides or thin films of FeSe [77,78].

This work consists of three main sections. In Sec. I, we introduce the RSW Hamiltonian, the relevant notation to study complex tensor order, and the Ginzburg-Landau theory for the d-wave superconducting state. In Sec. II, we analyze the strong-coupling phase transition for $\mu = 0$. In Sec. III, we eventually study the weak-coupling case, where $\mu > 0$ sets the largest energy scale in the system. We then summarize our findings and give an outlook in Sec. IV. Some of the more technical computations are presented in the Appendices.

I. MODEL

A. Rarita-Schwinger-Weyl Hamiltonian

We consider a three-dimensional electronic system whose low-energy single-particle excitations are described by the RSW Hamiltonian

$$H(\mathbf{p}) = \mathbf{p} \cdot \mathbf{J}, \tag{1}$$

with the 4×4 matrices J_i forming the spin-$\frac{3}{2}$ representation of the SO(3), $[J_i, J_j] = i\varepsilon_{ijk}J_k$. Here and in the following, we implicitly sum over repeated indices and denote $i = 1, 2, 3 = x, y, z$. In their standard representation, the spin matrices are given by

$$J_x = \frac{1}{2}\begin{pmatrix} 0 & \sqrt{3} & 0 & 0 \\ \sqrt{3} & 0 & 2 & 0 \\ 0 & 2 & 0 & \sqrt{3} \\ 0 & 0 & \sqrt{3} & 0 \end{pmatrix}, \tag{2}$$

TABLE I. Complex tensor (*d*-wave) orders resulting from the mean-field theory in Luttinger and Rarita-Schwinger-Weyl semimetals.

	Luttinger semimetals	RSW semimetals
Band structure	Fourfold quadratic band touching $H = (\mathbf{p} \cdot \mathbf{J})^2 - \frac{5}{4}p^2$	Fourfold linear band crossing $H = \mathbf{p} \cdot \mathbf{J}$
Strong coupling, $\mu = 0$	Superconducting uniaxial nematic state with line nodes	Superconducting uniaxial nematic state with full gap
Weak coupling, $\mu > 0$	C_{2z}-symmetric state with broken time-reversal symmetry and BF surfaces	Tetragonal-symmetric cyclic state with broken time-reversal symmetry and BF surfaces

$$J_y = \frac{i}{2} \begin{pmatrix} 0 & -\sqrt{3} & 0 & 0 \\ \sqrt{3} & 0 & -2 & 0 \\ 0 & 2 & 0 & -\sqrt{3} \\ 0 & 0 & \sqrt{3} & 0 \end{pmatrix}, \quad (3)$$

$$J_z = \frac{1}{2} \begin{pmatrix} 3 & 0 & 0 & 0 \\ 0 & 1 & 0 & 0 \\ 0 & 0 & -1 & 0 \\ 0 & 0 & 0 & -3 \end{pmatrix}. \quad (4)$$

The Hamiltonian in Eq. (1) is invariant under the SO(3) group of rotations. To determine its eigenvalues we may choose a frame such that $\mathbf{p} = (0, 0, p)$, which yields four bands with energies $+\frac{3}{2}p$, $+\frac{1}{2}p$, $-\frac{1}{2}p$, $-\frac{3}{2}p$. As shown, for instance, in Ref. [21], these bands carry Chern numbers $+3, +1, -1, -3$, respectively, so that the total monopole charge of the fourfold crossing point, defined as the sum of Chern numbers of the positive energy bands, is four.

Note that in contrast to, say, Dirac particles in graphene or Weyl fermions in Weyl semimetals, a single RSW band-crossing point need not imply a second RSW crossing point in the Brillouin zone. There merely need to be other topological band crossings (possibly of different type) which ensure that the total topological charge of the material is zero. For this reason we only assume the presence of a single fourfold band crossing in the following and neglect possible intervalley or nesting effects on the many-body state.

Assuming full rotation invariance as in Eq. (1) is typically too strong of a constraint for modeling realistic materials, which are only invariant under discrete point groups. However, the isotropic model provides a computationally advantageous approximation for systems with small cubic anisotropy, and is also known to be a good approximation when the effects of long-range interactions on the band structure are taken into account [55,58]. Furthermore, as we show in this work, the preferred superconducting ground states that appear at both weak and strong coupling fall into irreducible representations of the cubic group, and as such are feasible orders even for anisotropic systems. Our findings should therefore be meaningful beyond the rotation-invariant limit.

In order to quantify the deviation from full rotation invariance and to further elucidate the nature of the RSW band-crossing point, notice that the most general 4×4 Hamiltonian linear in $\mathbf{p}$ that is invariant under the cubic rotational group O is given by

$$\bar{H}(\mathbf{p}) = \sum_{i=1}^{3} p_i \left(J_i + c J_i^3 \right), \quad (5)$$

where c is a real parameter.[1] This generalized version of $\bar{H}(\mathbf{p})$ has been shown to emerge in critical antiperovskite Dirac materials [58,79], for various space-group symmetries in three-dimensional materials [9,17], or in transition metal silicides [10]. For $c \in [-\frac{4}{9}, -4]$, the band structure topology is different from $H(\mathbf{p})$ in Eq. (1), with the total monopole charge being -2. Furthermore, for $c = -\frac{4}{7}$ the single-particle sector acquires an enlarged Lorentz symmetry [58] and corresponds to two copies of Weyl Hamiltonians with equal chirality [9,21]. This distinguishes this limit from a massless Dirac Hamiltonian, which decomposes into two Weyl Hamiltonians with opposite chirality. The interplay between anisotropy, topology, and interactions leads to intriguing effects in RSW semimetals [21], but these are beyond the scope of this study. Hereafter, we consider only the fully rotation-invariant system.

B. Complex tensor order

The low-energy physics of interacting RSW fermions is assumed to be captured by the minimal Lagrangian

$$L = \psi^\dagger [\partial_\tau + H(\mathbf{p}) - \mu] \psi + g_1 (\psi^\dagger \psi)^2 + g_2 (\psi^\dagger \gamma_a \psi)^2, \quad (6)$$

which features rotation and time-reversal symmetry. Here, $\psi = (\psi_{3/2}, \psi_{1/2}, \psi_{-1/2}, \psi_{-3/2})^{\mathrm{T}}$ is a four-component Grassmann field, τ denotes imaginary time, $\mathbf{p} = -i\boldsymbol{\nabla}$ is the momentum operator, five 4×4 matrices γ_a satisfy the anticommuting Clifford algebra, $\{\gamma_a, \gamma_b\} = 2\delta_{ab}$, and summation over $a = 1, \dots, 5$ is implied. The Fermi velocity is set to unity. (The explicit expression of the γ matrices used here can be found in Appendix A.) We can choose $\gamma_{1,2,3}$ to be real and $\gamma_{4,5}$ to be complex, so that the time-reversal operator is given by $\mathcal{T} = \gamma_{45}\mathcal{K}$, where $\gamma_{ab} = i\gamma_a \gamma_b$ and $\mathcal{K}$ denotes complex conjugation. We assume that the RSW Hamiltonian captures the band structure of an underlying material for momenta below an ultraviolet cutoff Λ, which marks the scale at which the quadratic terms in the single-particle Hamiltonian begin to matter.

In the presence of rotation symmetry, the two four-fermion interaction terms in Eq. (6) constitute a Fierz-complete set of short-range interactions [6,26,80]. Any other local interaction terms necessarily contain derivatives and thus are suppressed for small μ. We neglect the long-range Coulomb interaction here, the subtle effects of which [5,6,24,26] may be, due to a sufficiently large dielectric constant, assumed to set in only

---

[1]We have $c = \frac{4(2-\alpha)}{13\alpha - 14}$ for α defined in Eq. (2) of Ref. [21].

at the length scales much longer than the superconducting coherence length. We can rewrite the interaction terms in Eq. (6) using the Fierz rearrangement formula as $L_s + L_d$ with [32,80]

$$L_s = g_s(\psi^\dagger \gamma_{45} \psi^*)(\psi^T \gamma_{45} \psi), \tag{7}$$

$$L_d = g_d(\psi^\dagger \gamma_a \gamma_{45} \psi^*)(\psi^T \gamma_{45} \gamma_a \psi). \tag{8}$$

The condensation of $\Delta_s = \langle \psi^T \gamma_{45} \psi \rangle$ or $\Delta_a = \langle \psi^T \gamma_{45} \gamma_a \psi \rangle$ corresponds to the onset of s- or d-wave superconductivity, respectively, and these two represent the complete set of local (momentum-independent) superconducting orders [32]. Explicit forms of Δ_a in terms of electronic operators are given in Ref. [40]. We have [32,80]

$$g_s = \tfrac{1}{4}(g_1 + 5g_2), \tag{9}$$

$$g_d = \tfrac{1}{4}(g_1 - 3g_2), \tag{10}$$

and so an attraction in the d-wave channel can be induced by a sufficiently positive value of g_2. In the following we assume $g_s = 0$ and $g_d = -g < 0$. We refer to Refs. [45,60] for the interplay of s-wave superconductivity with d-wave order in Luttinger semimetals. The five complex components of the object $\vec{\Delta} = (\Delta_1, \ldots, \Delta_5)$, directly by their definition, transform the same way as the five matrices γ_a under rotations. This is facilitated by the observation that the time-reversal operator $\mathcal{T} = \gamma_{45}\mathcal{K}$ commutes with rotations. γ_a, on the other hand, transform equivalently to the spherical harmonics of angular momentum of two [5,6,24,26]. We may therefore collect the five Δ_a into a matrix ϕ, which is an irreducible second-rank tensor under rotations, defined as

$$\phi_{ij} = \Delta_a M^a_{ij}. \tag{11}$$

The five real Gell-Mann matrices [26] M^a provide a basis of three-dimensional symmetric real traceless matrices. We choose the particular representation

$$\phi = \begin{pmatrix} \Delta_1 - \frac{1}{\sqrt{3}}\Delta_2 & \Delta_5 & \Delta_3 \\ \Delta_5 & -\Delta_1 - \frac{1}{\sqrt{3}}\Delta_2 & \Delta_4 \\ \Delta_3 & \Delta_4 & \frac{2}{\sqrt{3}}\Delta_2 \end{pmatrix}. \tag{12}$$

The Ginzburg-Landau free energy $F(\phi)$ for complex tensor order, invariant under $SO(3) \times U(1)$, is constrained by the following remarkable fact from invariant theory: Any expansion of $F(\phi)$ in powers of ϕ that is invariant under $\phi \to R\phi R^T$ can only depend on the *eight* invariants

$$I_1 = \text{tr}(\phi^\dagger \phi), \quad I_2 = \text{tr}(\phi^2), \quad I_3 = \text{tr}(\phi^{\dagger 2}),$$

$$I_4 = \text{tr}(\phi^3), \quad I_5 = \text{tr}(\phi^{\dagger 3}), \quad I_6 = \text{tr}(\phi^2 \phi^\dagger), \tag{13}$$

$$I_7 = \text{tr}(\phi^{\dagger 2} \phi), \quad I_8 = \text{tr}(\phi^\dagger \phi \phi^\dagger \phi),$$

which are the integrity basis of $SO(3)$. Imposing also $U(1)$ symmetry, the terms $\mathcal{O}_n$ that can appear to nth order in ϕ, with $n \leqslant 6$, are

$$\mathcal{O}_2 = \{I_1\}, \tag{14}$$

$$\mathcal{O}_4 = \{I_1^2, I_2 I_3, I_8\}, \tag{15}$$

$$\mathcal{O}_6 = \{I_1^3, I_1 I_2 I_3, I_4 I_5, I_6 I_7, I_1 I_8\}, \tag{16}$$

and, importantly, for n_o odd we have

$$\mathcal{O}_{n_o} = \varnothing. \tag{17}$$

These constraints result in a significant reduction of allowed terms in the GL free energy and thus a substantial computational simplification. For example, the seemingly distinct quartic term $\text{tr}(\phi^\dagger \phi^\dagger \phi \phi)$ is actually a linear combination of the three quartic terms in $\mathcal{O}_4$.

Of course, since $SO(3)$ has a unique irreducible complex five-dimensional representation, an equivalent way of thinking about the d-wave order parameter is as of a (pure, macroscopic) quantum state in the spin-2 Hilbert space. The five real Gell-Mann matrices then transform into each other under $SO(3)$ as the following linear combinations of the standard basis:

$$|M_1\rangle = \frac{1}{\sqrt{2}}(|-2\rangle + |2\rangle), \tag{18}$$

$$|M_2\rangle = |0\rangle, \tag{19}$$

$$|M_3\rangle = \frac{1}{\sqrt{2}}(|-1\rangle - |1\rangle), \tag{20}$$

$$|M_4\rangle = \frac{i}{\sqrt{2}}(|-1\rangle + |1\rangle), \tag{21}$$

$$|M_5\rangle = \frac{i}{\sqrt{2}}(|-2\rangle - |2\rangle), \tag{22}$$

which we label the same way as the matrices to emphasize their identical transformation law under rotations. Here, $J_z|m\rangle = m|m\rangle$ and $m = 0, \pm 1, \pm 2$. Note that each state $|M_a\rangle$ is defined to be invariant under time reversal, which is then simply complex conjugation of the coefficients of the state when expressed in this basis. One can therefore write an order parameter equivalently in this *real* basis as a state, defined as $|\vec{\Delta}\rangle = \Delta_a|M_a\rangle$.

We may also note that the states $|M_{1,2}\rangle$ constitute the "E" two-dimensional irreducible representation of the cubic group, whereas the remaining $|M_{3,4,5}\rangle$ constitute the "T_2" three-dimensional irreducible representation of the cubic group.

From the above definition of the real (time-reversal-invariant) basis one readily infers that the first invariant above is

$$I_1 = 2\Delta_a^* \Delta_a = 2\langle \vec{\Delta}|\vec{\Delta}\rangle, \tag{23}$$

i.e., simply the norm of the state, whereas the next one,

$$I_3 = I_2^* = 2\Delta_a^* \Delta_a^* = 2\langle \vec{\Delta}|\mathcal{K}|\vec{\Delta}\rangle, \tag{24}$$

is the overlap between the state and its time-reversed copy. A bit more algebra shows that the square of the average angular momentum, which is proportional to the magnetization, is

$$\sum_{i=1}^3 \langle \vec{\Delta}|J_i|\vec{\Delta}\rangle^2 = \frac{3}{2}I_8 - \frac{1}{2}I_1^2 - \frac{1}{4}|I_2|^2 = \frac{1}{2}\text{tr}([\phi, \phi^*]^2) \tag{25}$$

with $[\ldots, \ldots]$ as the commutator. The last equation demonstrates two things: (1) any real order parameter has zero average angular momentum, i.e., magnetization, (2) the three

independent $SO(3) \times U(1)$ quartic terms in the Ginzburg-Landau free energy are linear combinations of the norm of the state, the $SO(3)$-invariant measure of time-reversal symmetry breaking exhibited by the state, and its average magnetization (angular momentum).

Let us now define some of the states that will play a prominent role in the mean-field Ginzburg-Landau theory that will be discussed shortly. First, if the state is real, the matrix ϕ can always be transformed by a rotation and a phase transformation into a diagonal form

$$\phi = \Delta_1 M_1 + \Delta_2 M_2 \qquad (26)$$

with real $\Delta_{1,2}$. If $\Delta_1 \neq 0$, this is the biaxial nematic state, which can be at most D_4 symmetric, when $\Delta_2 = 0$ [81]. If, on the other hand, $\Delta_1 = 0$, this is the uniaxial nematic state, which is invariant under the continuous subgroup $SO(2)$ of rotations about one of the axis of the reference frame, and under rotations by π around any orthogonal axis. As already mentioned, the average magnetization (angular momentum) of any real state is zero.

The normalized state which breaks time-reversal symmetry maximally and shows the maximal average angular momentum of 2 is the ferromagnetic state. In the matrix notation it reads as

$$\phi = \frac{\Delta}{\sqrt{2}}(M_1 + iM_5) \qquad (27)$$

with Δ real, or $|\vec{\Delta}\rangle = \Delta|2\rangle$ in the quantum notation. This state is also invariant under the $SO(2)$ subgroup of rotations.

Finally, in the spin-2 Hilbert space there exists a state which maximally breaks time-reversal symmetry, but nevertheless has vanishing average magnetization. This is the "cyclic state," which in the matrix notation can be written as

$$\phi = \frac{\Delta}{\sqrt{2}}(M_1 + iM_2) \qquad (28)$$

with Δ real. One can show that this state is invariant under the tetragonal group T [81], which is the largest discrete subgroup of the $SO(3)$ that can be realized in the spin-2 Hilbert space. Its uniqueness, up to an $U(1)$ and $SO(3)$ transformation, follows from the observation that after the real part of the complex tensor order parameter is diagonalized, it can always be made to be proportional only to the matrix M_1 by a suitable $U(1)$ transformation. In order for the state to break time reversal maximally, the imaginary part of the tensor can then contain only the components M_a with $a \neq 1$, and be of the same norm as the real part. The only such component that commutes with M_1 and by the formula in Eq. (25) would yield vanishing magnetization of the state is then M_2, which then implies the specific form of the cyclic state given above.

Another way to understand the uniqueness of the cyclic state is to use the Majorana representation of the spin-2 states in terms of four points on the unit sphere, and realize that, modulo an overall rotation, there is a unique way to arrange them in a tetragonally symmetric way [81].

C. Ginzburg-Landau theory

In this section, we present the Ginzburg-Landau expansion of the free energy near the second-order phase transition
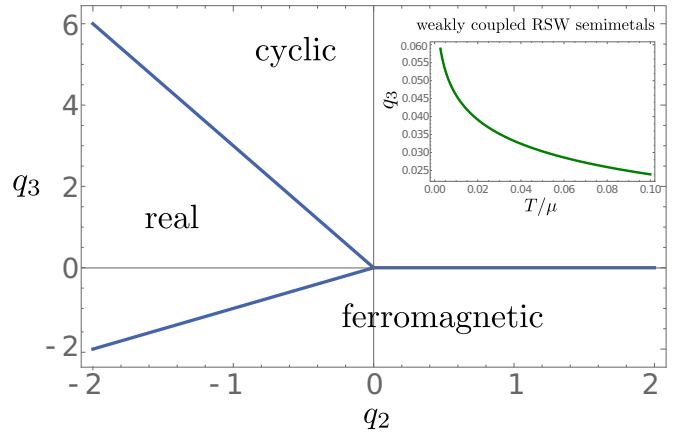

FIG. 1. The phase diagram of a three-dimensional *d*-wave superconductor is determined by the coefficients q_2 and q_3 (in arbitrary units) of the quartic terms in the Ginzburg-Landau expansion. The inset shows the q_3 as a function of temperature in the weak-coupling regime. Positivity of both q_2 and q_3 implies that the cyclic state is the preferred superconducting order at finite chemical potential.

toward *d*-wave order. In the first part we discuss how the values of the coefficients of the quartic terms in the free energy determine the superconducting state and derive the corresponding phase diagram shown in Fig. 1. This phase diagram was first obtained by Mermin [61], and we rederive it and elaborate on it here as it is needed for further presentation. In the second part we show how the coefficients in the Ginzburg-Landau free energy can be computed for the weakly coupled RSW semimetal.

1. Phase diagram

Close to a second-order phase transition, we can expand the free energy $F(\vec{\Delta})$ for a uniform *d*-wave order parameter according to

$$F(\vec{\Delta}) = F_2(\vec{\Delta}) + F_4(\vec{\Delta}) + \mathcal{O}(\phi^6), \qquad (29)$$

with the quadratic and the quartic terms

$$F_2(\vec{\Delta}) = r|\vec{\Delta}|^2, \qquad (30)$$

$$F_4(\vec{\Delta}) = q_1|\vec{\Delta}|^4 + q_2|\vec{\Delta}^2|^2 + \frac{q_3}{2}I_8. \qquad (31)$$

The ordered phase as usual corresponds to $r < 0$. Crucially, although ϕ is a second-rank tensor under rotations, no cubic term is allowed due to the additional global $U(1)$ symmetry in the problem. Depending on the signs and relative magnitudes of q_1, q_2, and q_3, either real order, the cyclic state, or the ferromagnetic state yield the lowest free energy (see Fig. 1). For Luttinger semimetals, $q_3 = 0$ at the mean-field level, which leaves a large accidental degeneracy, broken only by the sextic terms [40,61]. For RSW semimetals, however, we will find shortly that q_3 is finite in general, even at the level of the one-loop approximation.

Some intuition on the interplay of the coefficients in Eq. (31) can be gained by setting $q_3 = 0$. In order to have a stable potential bounded from below, we require $q_1 > 0$, and so the sign of q_2 determines the nature of the superconducting ground state: for $q_2 < 0$, a maximal value of $|\vec{\Delta}^2|$ leads to

the largest decrease of the free energy in the superconducting state. This implies that $\vec{\Delta}$ is real (up to an overall phase factor) and thus preserves time-reversal symmetry. In contrast, for $q_2 > 0$, a minimal value of $|\vec{\Delta}^2|$ is favorable, which is readily solved by any genuinely complex order parameter satisfying $\vec{\Delta}^2 = 0$. Such states satisfy $\text{tr}(\phi^2) = 0$ and break time-reversal symmetry maximally, that is, time-reversal transformation makes them orthogonal to themselves [Eq. (24)]. As we already noted, both the cyclic and the ferromagnetic state break time-reversal symmetry maximally, as well as infinitely many other states.

If $q_2 > 0$ and the breaking of time reversal is preferred in the superconducting state, Eq. (25) shows that the sign of q_3 decides whether the state should or should not exhibit a finite average of the angular momentum, i.e., of magnetization. For $q_3 < 0$, maximal average magnetization is preferred and the ferromagnetic state with the maximal value of $I_8 = 4$ ensues. In the opposite case of $q_3 > 0$, the average magnetization of the superconducting state should be minimal, although time-reversal symmetry is maximally broken. The cyclic state with minimal value of $I_8 = \frac{4}{3}$, which is tantamount to zero average magnetization, is then the result of these two simultaneous requirements. The phase diagram implied by the quartic terms of the Ginzburg-Landau theory is given in Fig. 1.

Importantly, for any real order parameter we have $F_4(\vec{\Delta}) = (q_1 + q_2 + q_3)\vec{\Delta}^4$ in Eq. (31). This remains true even if the coefficients $q_{1,2,3}$ are determined beyond the mean-field approximation. As a result, the expansion of the free energy to quartic order can never decide which particular real order is chosen among the many possible real states $\vec{\Delta} \in \mathbb{R}^5$. To find the optimal real state that minimizes the free energy, one would have to work with the full expression for the function $F(\vec{\Delta})$. However, expanding the latter to sextic order in the field gives a good approximation to the optimal state near critical temperature, as was shown explicitly for the BCS d-wave state at zero temperature in Ref. [60]. The most general terms for complex tensor order to sextic order read as

$$F_6(\vec{\Delta}) = s_1|\vec{\Delta}|^6 + s_2|\vec{\Delta}|^2|\vec{\Delta}^2|^2 + s_3|\text{tr}(\phi^3)|^2$$
$$+ s_4|\text{tr}(\phi^2\phi^\dagger)|^2 + \frac{s_5}{2}|\vec{\Delta}|^2 I_8. \quad (32)$$

In particular, for real order parameters we have $F_6(\vec{\Delta}) = (s_1 + s_2 + s_5)\vec{\Delta}^6 + (s_3 + s_4)(\text{tr}\phi^3)^2$, and so the sign of $s_3 + s_4$ determines whether the uniaxial nematic state, with maximal $|\text{tr}(\phi^3)| > 0$, or the biaxial state, with minimal $|\text{tr}(\phi^3)| = 0$ is energetically favorable.

2. Computation of the coefficients

The values of the coefficients entering the expansion of the free energy may be determined in the following way. We first compute the free-energy expansion to quartic order in the field. Within the mean-field approximation we have

$$F_2(\vec{\Delta}) = \frac{1}{g}|\vec{\Delta}|^2 - \frac{1}{2}K_{ab}\Delta_a^*\Delta_b, \quad (33)$$

$$F_4(\vec{\Delta}) = \frac{1}{4}K_{abcd}\Delta_a^*\Delta_b\Delta_c^*\Delta_d \quad (34)$$

with

$$K_{ab} = \text{tr}\int_Q^\Lambda G_0(\omega_n, \mu, \mathbf{q})\gamma_a G_0(-\omega_n, \mu, \mathbf{q})\gamma_b, \quad (35)$$

$$K_{abcd} = \text{tr}\int_Q^\Lambda G_0(\omega_n, \mu, \mathbf{q})\gamma_a G_0(-\omega_n, \mu, \mathbf{q})\gamma_b$$
$$\times G_0(\omega_n, \mu, \mathbf{q})\gamma_c G_0(-\omega_n, \mu, \mathbf{q})\gamma_d. \quad (36)$$

Here, $\omega_n = (2n+1)\pi T$ denotes the fermionic Matsubara frequency with temperature T and the integration comprises

$$\int_Q^\Lambda := T\sum_{n\in\mathbb{Z}}\int_{\mathbf{q}}^\Lambda := T\sum_{n\in\mathbb{Z}}\int_{q\leqslant\Lambda}\frac{d^3q}{(2\pi)^3} \quad (37)$$

with ultraviolet cutoff $\Lambda \gg T, \mu$. The 4×4 Gaussian propagator reads as

$$G_0(\omega_n, \mu, \mathbf{p})$$
$$= (i\omega_n\mathbb{1} + H(\mathbf{p}) - \mu\mathbb{1})^{-1}$$
$$= \frac{[-i(\omega_n + i\mu)\mathbb{1} + H(\mathbf{p})]\{[(\omega_n+i\mu)^2+\frac{5}{2}p^2]\mathbb{1} - H(\mathbf{p})^2\}}{[(\omega_n + i\mu)^2 + \frac{1}{4}p^2][(\omega_n + i\mu)^2 + \frac{9}{4}p^2]}. \quad (38)$$

In order to determine the coefficients $q_{1,2,3}$ we then insert the states $\vec{\Delta}_1 = \Delta(0, 1, 0, 0, 0)$, $\vec{\Delta}_2 = \frac{\Delta}{\sqrt{2}}(1, i, 0, 0, 0)$, $\vec{\Delta}_3 = \frac{\Delta}{\sqrt{2}}(0, 0, 1, i, 0)$, and match them with

$$F_4(\vec{\Delta}_1) = (q_1 + q_2 + q_3)\Delta^4, \quad (39)$$

$$F_4(\vec{\Delta}_2) = \left(q_1 + \frac{2}{3}q_3\right)\Delta^4, \quad (40)$$

$$F_4(\vec{\Delta}_3) = (q_1 + q_3)\Delta^4. \quad (41)$$

The explicit expressions for the coefficients are summarized in Appendix C.

D. Energy spectrum of the quasiparticles

The energy spectrum of quasiparticles has the deciding influence on the low-energy properties of superconductors. For example, line nodes in the quasiparticle excitation spectrum lead to a linear temperature dependence of the London penetration depth or the thermal conductivity. The energy spectrum of the quasiparticles is defined by the Bogoliubov–de Gennes (BdG) Hamiltonian

$$H_{\text{BdG}}(\mathbf{p}) = \begin{pmatrix} H(\mathbf{p}) - \mu\mathbb{1} & \Delta_a\gamma_a \\ \Delta_a^*\gamma_a & -[H(\mathbf{p}) - \mu\mathbb{1}] \end{pmatrix}, \quad (42)$$

which should be understood as acting on the Nambu (eight-component) spinor $(\psi, \mathcal{T}\psi)^{\text{T}}$. Recalling that $\mathcal{T}^{-1}H(\mathbf{p})\mathcal{T} = H^{\text{T}}(-\mathbf{p})$, the lower (hole) block reduces to the standard expression. In order to understand the main properties of the spectrum, let us then consider a generic case without time-reversal symmetry,

$$H_{\text{BdG}} = \sigma_3 \otimes [H(\mathbf{p}) - \mu\mathbb{1}] + \Delta_1\sigma_1 \otimes \gamma_a + \Delta_2\sigma_2 \otimes \gamma_b, \quad (43)$$

with γ_a and γ_b as any of the five γ matrices, with $a \neq b$. $\Delta_{1,2}$ are real. Since both $H(\mathbf{p})$ and all γ_a are even under time reversal, the first two terms of the Hamiltonian also respect time-reversal symmetry, i.e., $[\sigma_3 \otimes (H(\mathbf{p}) - \mu\mathbb{1}), \mathbb{1} \otimes \mathcal{T}] = [\sigma_1 \otimes \gamma_a, \mathbb{1} \otimes \mathcal{T}] = 0$. The last term by virtue of involving the imaginary matrix σ_2, on the other hand, breaks time-reversal symmetry, and $\{\sigma_2 \otimes \gamma_b, \mathbb{1} \otimes \mathcal{T}\} = 0$. Although the above H_{BdG} by construction breaks time reversal, one can use the antiunitary $\mathcal{T}$ to construct the operator $\mathcal{A} = \sigma_2 \otimes \mathcal{T}$, which anticommutes with all three terms in the BdG Hamiltonian, and therefore $\{H_{\text{BdG}}, \mathcal{A}\} = 0$. This, of course, only means that H_{BdG} has a spectrum symmetric around zero, which is the well-known particle-hole symmetry inherent to Nambu's construction and any superconducting state.

Since the time-reversal operator $\mathcal{T}$ inverts the momentum $\mathbf{p}$ in the electron Hamiltonian $H(\mathbf{p})$, this, as well known, also means that the eigenstates of H_{BdG} at opposite momenta are related by the operator $\mathcal{A}$, and that the corresponding eigenvalues are similarly related as

$$E(-\mathbf{p}) = -E(\mathbf{p}). \tag{44}$$

Were the $H(\mathbf{p})$ also inversion symmetric, the particle-hole symmetry would imply that at any fixed momentum there are pairs of eigenstates of H_{BdG} which differ only in sign of otherwise identical dispersion. The determinant of the Hamiltonian at any momentum, $\det H_{\text{BdG}}(\mathbf{p}) = \prod_{n=1}^{8} E_n(\mathbf{p})$, would then be $\det H_{\text{BdG}}(\mathbf{p}) = \prod_{n=1}^{4} (-E_n^2(\mathbf{p}))$, and evidently non-negative. The important insight of Ref. [36] was to recognize that in this situation one can nevertheless define and consider the Pfaffian, which may change sign, and thus lead to a Bogoliubov-Fermi (BF) surface of zero energy. In the case of RSW fermions with $H(\mathbf{p}) = \mathbf{p} \cdot \mathbf{J}$, the inversion symmetry is however absent, and the particle-hole symmetry by itself does not imply that for fixed momentum $\mathbf{p}$ the spectrum has to be symmetric around zero. The determinant of the Hamiltonian at a fixed momentum is therefore not automatically non-negative. We further show in the Appendix that there is actually no other operator, linear or antilinear, that would anticommute with the BdG Hamiltonian for RSW fermions if the momentum is treated as an arbitrary parameter unaffected by the transformation, when the time-reversal symmetry is broken. The determinant therefore is actually free to change sign as a function of momentum. This permitted change of the sign of the determinant itself also allows for the appearance of a BF surface. This is what we find to be the case in explicit calculations that follow.

We may observe an additional symmetry of $H_{\text{BdG}}(\mathbf{p})$ that arises at $\mu = 0$. When $H(\mathbf{p})$ respects time reversal $\mathcal{T}$ but violates inversion $\mathcal{I}$, it is odd under their combination $\mathcal{I}\mathcal{T}$. [This is the same as saying that $H(\mathbf{p})$ becomes odd under $\mathcal{T}$ if the momentum is treated as a parameter unaffected by the transformation, as discussed above.] We may now form a new antilinear operator $\mathcal{B} = \sigma_1 \otimes \mathcal{I}\mathcal{T}$, and observe that, since all γ_a are even under inversion as well, the entire $H_{\text{BdG}}(\mathbf{p})$ commutes with it, provided $\mu = 0$. When $\mu \neq 0$ the extra term $\mu\sigma_3 \otimes \mathbb{1}$ anticommutes with $\mathcal{B}$, and the symmetry is violated. Since $\mathcal{B}^2 = -1$, however, all the eigenstates at fixed momentum and at $\mu = 0$ will be doubly degenerate, due to
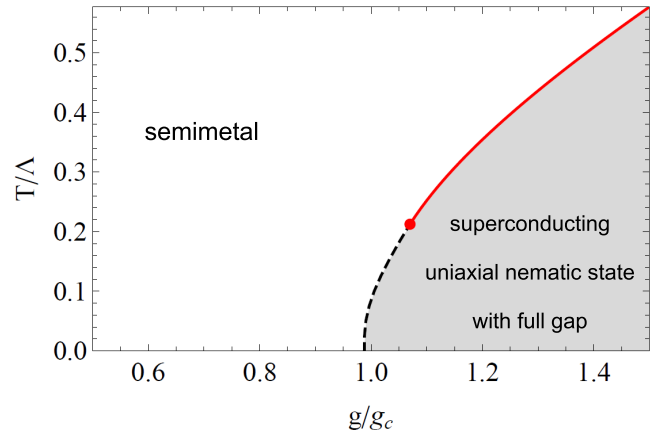

FIG. 2. Mean-field phase diagram for complex tensor order in RSW semimetals for $\mu = 0$. We observe a strong-coupling phase transition toward the superconducting state with time-reversal symmetric uniaxial nematic order parameter and full gap. The solid red and dashed black lines, respectively, correspond to a second- and first-order phase transition, with the tricritical point located at $(g/g_c, T_c/\Lambda) = (1.07, 0.20)$. Here, Λ is the ultraviolet cutoff of the otherwise seemingly scale-invariant system. We define $g_c = 6\pi^2/\Lambda^2$ as a reference coupling.

Kramers theorem. This will be confirmed in explicit calculations (see Fig. 3). An implication is that for $\mu = 0$ the determinant $\det H_{\text{BdG}}(\mathbf{p}) = \prod_{n=1}^{8} E_n(\mathbf{p}) = (\prod_{n=1}^{4} E_n(\mathbf{p}))^2$, and becomes non-negative. Nevertheless, we will find that it may be still be zero on a BF surface in some, but not all, superconducting states.

II. STRONG-COUPLING PHASE TRANSITION

We now determine the phase diagram for the chemical potential at the Fermi point ($\mu = 0$). Weak short-range interactions are irrelevant due to the vanishing density of states at the band-crossing point. However, for strong enough coupling, interactions induce a phase transition into a complex tensor ordered state. We show that the energetically preferred configuration is the real uniaxial nematic state with full gap.

A. Phase diagram

In order to determine the phase diagram for $\mu = 0$ we first expand the mean-field Ginzburg-Landau free energy $F(\vec{\Delta})$ to sextic order in powers of the field ϕ. This yields a strong-coupling second-order phase transition at nonzero temperature. The line of second-order transitions terminates at a tricritical point, where the transition turns first order and the expansion becomes meaningless (see Fig. 2). This second-order phase transition line in the plane T/Λ vs g/g_c, with $g_c = 6\pi^2/\Lambda^2$, is determined from solving $r = r(g, T, \Lambda) = 0$, where the coefficient r was defined in Eqs. (30) and (33). At the transition point, the quartic coefficients q_i in the free-energy expansion are such that the symmetry-breaking order parameter is real. A stable second-order transition then requires the quartic coefficient $q_1 + q_2 + q_3$ to be positive. From the explicit expressions we find that the second-order line terminates at a tricritical point located at $(g/g_c, T_c/\Lambda) =$

(a) uniaxial nematic state

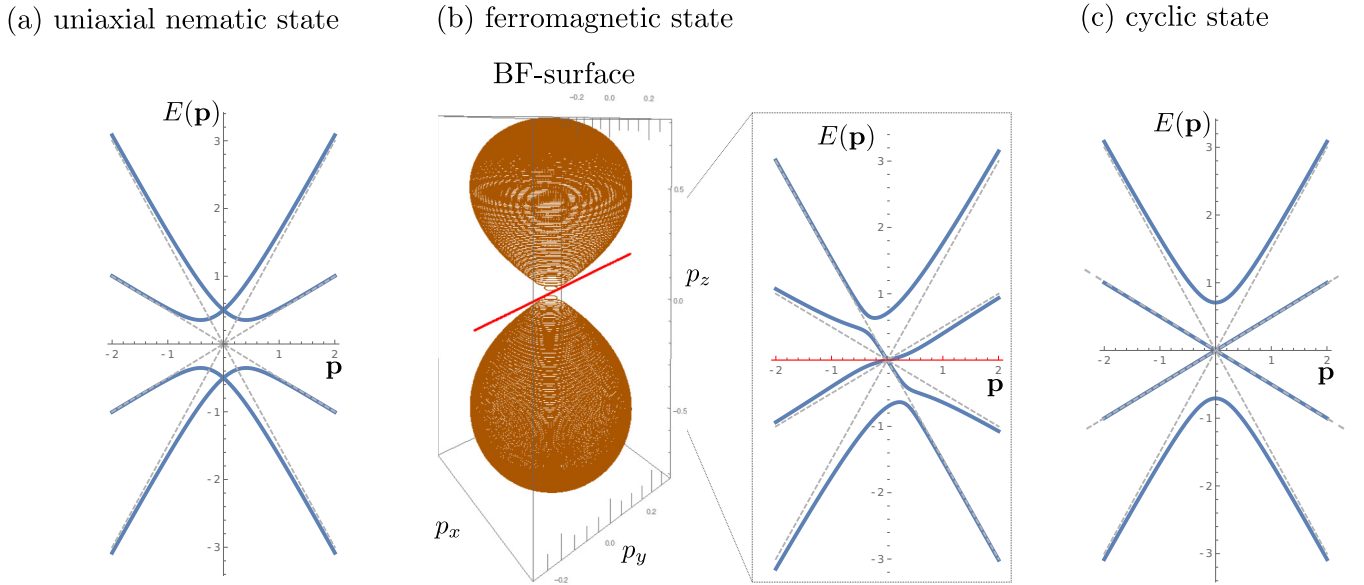(b) ferromagnetic state

(c) cyclic state

FIG. 3. Energy dispersion of quasiparticles in competing superconducting states in the strong-coupling regime for $\mu = 0$. We plot the energy along the (1,1,1)-momentum direction for different states with $\Delta = 0.5$, in units of the cutoff Λ. (a) Depicts the energetically preferred uniaxial nematic state whose energy spectrum is fully gapped. The superconducting states with broken time-reversal symmetry exhibit a closed dumbbell-like Bogoliubov-Fermi surface, in the ferromagnetic state, or a point node, as in the cyclic state. The gray, dashed lines in the energy spectrum denote the energy in the normal state. The red line in (b) depicts the momentum direction (1,1,1) along which the energy dispersion of the ferromagnetic state is plotted. The spectrum in the cyclic state plotted in (c) is actually rotationally symmetric. All the spectra at $\mu = 0$ are doubly (Kramers) degenerate, as discussed in the text.

(1.07, 0.20). At lower temperatures, the phase transition becomes first order, as we discuss below.

In order to determine the real order parameter that develops at the second-order transition, we compute the sextic order coefficients in Eq. (32) from

$$F_6(\vec{\Delta}) = -\frac{1}{6} K_{abcdef} \Delta_a^* \Delta_b \Delta_c^* \Delta_d \Delta_e^* \Delta_f \qquad (45)$$

with

$$K_{abcdef} = \text{tr} \int_Q G_0(\omega_n, \mathbf{q}) \gamma_a G_0(-\omega_n, \mathbf{q}) \gamma_b G_0(\omega_n, \mathbf{q}) \gamma_c$$
$$\times G_0(-\omega_n, \mathbf{q}) \gamma_d G_0(\omega_n, \mathbf{q}) \gamma_e G_0(-\omega_n, \mathbf{q}) \gamma_f \qquad (46)$$

through a matching analogous to Eqs. (39)–(41) (see Ref. [40]). The resulting expressions for $s_{1,\dots,5}$ are summarized in Appendix C. We find that $s_3 + s_4$ is always negative, so that the uniaxial nematic state with maximal $\text{tr}(\phi^3) > 0$ is energetically favored.

Below the tricritical point, the phase transition is of first order and the transition line cannot be obtained from an expansion of the mean-field free energy. Instead, for $T/\Lambda < 0.20$, we employ the full expression for the mean-field free energy that follows from the quasiparticle energies for real orders. The latter are the eigenvalues of the BdG Hamiltonian at charge neutrality

$$H_{\text{BdG}}(\mathbf{p}) = \begin{pmatrix} H(\mathbf{p}) & \Delta_a \gamma_a \\ \Delta_a^* \gamma_a & -H(\mathbf{p}) \end{pmatrix}. \qquad (47)$$

For the most general real order $\vec{\Delta} = (\Delta_1, \Delta_2, 0, 0, 0)$ we find doubly degenerate eigenvalues $E_\pm(\mathbf{p}), -E_\pm(\mathbf{p})$, with

$$E_\pm(\mathbf{p}) = \left[\frac{5}{4} p^2 + \vec{\Delta}^2 \pm \left[p^2(p^2 + 2\vec{\Delta}^2) \right.\right.$$
$$\left.\left. + 4\Delta_1 \Delta_2 d_1(\mathbf{p}) + 2(\Delta_1^2 - \Delta_2^2) d_2(\mathbf{p}) \right]^{1/2} \right]^{1/2}, \quad (48)$$

$d_1(\mathbf{p}) = \sqrt{3}(p_x^2 - p_y^2)/2$, $d_2(\mathbf{p}) = (2p_z^2 - p_x^2 - p_y^2)/2$. We label the positive eigenvalues as $E_{1,2} = E_+$ and $E_{3,4} = E_-$. The mean-field free energy is then given by

$$F(\vec{\Delta}) = \frac{1}{g} |\vec{\Delta}|^2 - \frac{1}{2} \sum_{\nu=1}^{4} \int_{\mathbf{q}}^{\Lambda} [|E_\nu(\mathbf{q}, \vec{\Delta})|$$
$$+ 2T \ln(1 + e^{-|E_\nu(\mathbf{q}, \vec{\Delta})|/T})]. \qquad (49)$$

We verify that the uniaxial configuration ($\Delta_1 = 0$) has a lower free energy than the biaxial configuration ($\Delta_2 = 0$). The resulting phase diagram including both first- and second-order transitions is shown in Fig. 2.

B. Nodal structure of the gap

The nodal structure of the gap is of critical importance for low-energy transport in the superconducting state, as already noted. Furthermore, the optimal order parameter is typically such that nodes of the gap are minimized and thus a knowledge of the nodal structure of competing order parameters helps to understand the superconducting ground state.

We first show that the uniaxial nematic state has a full gap, i.e., it is without nodes. For this we compute the determinant

of H_{BdG} in Eq. (47) for the uniaxial nematic state. We find

$$\det(H_{\text{BdG}}(\mathbf{p}))_{\text{uniaxial}} = \frac{1}{256}(9p^4 + 16\Delta^2(p^2 + \Delta^2)$$
$$+ 24p^2\Delta^2 \cos(2\theta_{\mathbf{p}}))^2, \qquad (50)$$

with $\mathbf{p} = p(\sin\theta_{\mathbf{p}} \cos\varphi_{\mathbf{p}}, \sin\theta_{\mathbf{p}} \sin\varphi_{\mathbf{p}}, \cos\theta_{\mathbf{p}})$. Since the determinant is the product of all quasiparticle energies in Eq. (48), a node in any of the eigenvalues at a certain momentum $\mathbf{p}$ would imply a zero of the determinant. We easily verify, however, that the determinant is always strictly positive: even for θ such that $\cos(2\theta) = -1$, there is no real solution p of $9p^4 + 16\Delta^2(p^2 + \Delta^2) - 24p^2\Delta^2 = 0$. The resulting energy dispersion of these quasiparticles along the $(1,1,1)$ momentum direction and the gap in the energy spectrum are shown in Fig. 3(a).

From the analysis of the nodal structure of the gap we can further understand why time-reversal symmetry-breaking states, such as the cyclic state or the ferromagnetic state, are disfavored for $\mu = 0$. For this note that a suitable superconducting order parameter should gap out the linear band crossing at $p = 0$. However, inserting $\mathbf{p} = 0$ into the most general form of H_{BdG} in Eq. (47) we find

$$\det(H_{\text{BdG}}(\mathbf{p} = 0)) = |\vec{\Delta}^2|^4. \qquad (51)$$

Consequently, states with $\vec{\Delta}^2 = 0$, such as, for instance, the ferromagnetic and cyclic state in Figs. 3(b) and 3(c), do not open a gap at the crossing point and so are energetically inferior in comparison to real order parameters.

The cyclic state exhibits a point node where the $\frac{1}{2}$-energy bands are crossing and only the $\frac{3}{2}$-energy bands of the normal states are gapped out by the superconducting pairing mechanism, as shown in Fig. 3(c). Interestingly, the quasiparticle spectrum in the cyclic state happens to be also fully rotationally, and even symmetric around zero energy at fixed momentum. For the ferromagnetic state, we find BF surfaces centered around zero momentum. The corresponding energy spectrum is not symmetric around zero energy at fixed momentum, but of course displays the general particle-hole symmetry $E(\mathbf{p}) = -E(-\mathbf{p})$, as can be seen in Fig. 3(b). All the spectra at $\mu = 0$ exhibit the Kramers degeneracy at any momentum, as discussed earlier.

III. WEAK-COUPLING PHASE TRANSITION

We turn next to the phase diagram for finite chemical potential ($\Lambda \gg \mu > 0$) in the weak-coupling regime. For finite chemical potential, the normal state features two spherical Fermi surfaces with radii $p_1 = 2\mu/3$ and $p_2 = 2\mu$. Ideally, these Fermi surfaces of the normal state should be gapped out maximally in the superconducting state. We demonstrate that the uniaxial nematic state builds up line nodes at weak coupling, and that the energetically optimal configuration is the cyclic state, which breaks time-reversal symmetry and exhibits small BF surfaces.

A. Phase diagram

Due to the nonzero value of the chemical potential μ, two BCS-like instabilities occur at $p_1 = 2\mu/3$ and at $p_2 = 2\mu$
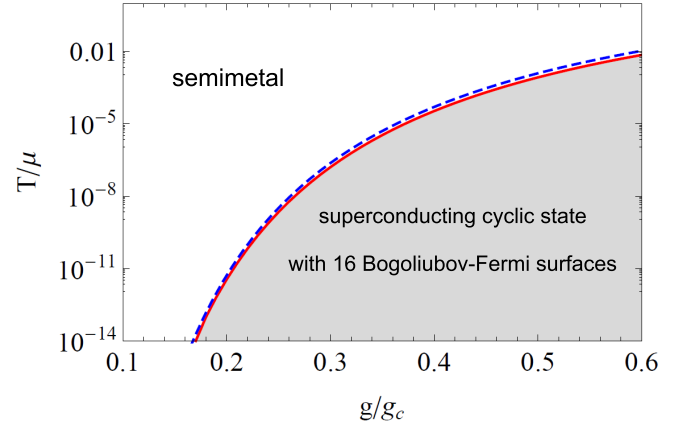

FIG. 4. Phase diagram for complex tensor order in RSW semimetals with finite chemical potential $\mu > 0$. The red line shows the critical temperature for the usual BCS-like weak-coupling second-order transition, the blue dashed line is the approximate formula from Eq. (52), both extrapolated here to strong coupling. The phase transition is toward the superconducting cyclic state, which breaks time-reversal symmetry maximally, has vanishing magnetic moment, and features 16 BF surfaces. For the plot we have chosen $\Lambda/\mu = 4$.

for arbitrarily weak attractive coupling $g > 0$. This leads to a second-order phase transition at the critical temperature

$$\frac{T_c(g)}{\mu} \simeq \exp\left[-\frac{45}{112}\frac{\Lambda^2}{\mu^2}\left(\frac{g_c}{g} - 1 + a\frac{\mu^2}{\Lambda^2}\right)\right], \qquad (52)$$

where $a = 0.613$. The corresponding phase diagram for $\Lambda/\mu = 4$ is shown in Fig. 4. In order to determine the concomitant superconducting state, we compute the coefficients $q_{1,2,3}$ from mean-field theory and read off the order parameter from the phase diagram in Fig. 1.

In the following, we present the leading terms in the expansions of $q_{1,2,3}$ in the weak-coupling regime, at temperatures $T \leqslant T_c \ll \mu$. Derivation is given in Appendix C 2, which also contains the exact expressions in terms of frequency and momentum integrals. We find that q_1 is positive and has the form

$$q_1 = \frac{2^{5/3}}{12153^{1/6}\pi}\frac{1}{t^2} + \frac{13}{945\pi^2}\ln(t) + O(t^0), \qquad (53)$$

with $t = T/\mu$ the small parameter near and below T_c. This implies that the potential is stable and bounded from below. The values of the coefficients q_2 and q_3 then select the superconducting state. These coefficients read as

$$q_2 = \frac{2^{2/3}}{12153^{1/6}\pi}\frac{1}{t^2} + \frac{22}{189\pi^2}\ln(t) + O(t^0) \qquad (54)$$

and

$$q_3 = -\frac{31}{315\pi^2}\ln(t) + O(t^0). \qquad (55)$$

(a) uniaxial nematic state
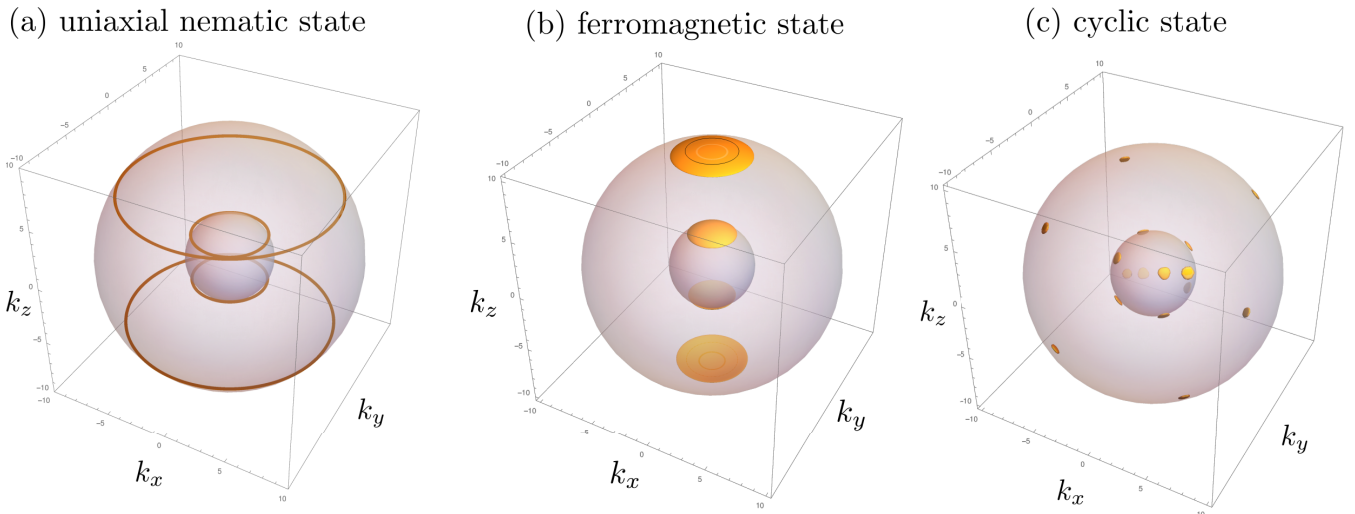
(b) ferromagnetic state

(c) cyclic state

FIG. 5. Nodal structure of quasiparticles in the weak-coupling regime, for $\mu/\Delta = 5$. The two spheres indicate the Fermi surfaces of the normal state with radii $p_1 = 2\mu/3$ and $p_2 = 2\mu$. The real uniaxial nematic state exhibits four line nodes, which constitute two groups of parallel circles and preserve SO(2) symmetry. The time-reversal symmetry-breaking ferromagnetic state displays four thin closed surfaces along the (0,0,1) direction, also featuring SO(2) symmetry. The cyclic states exhibits 16 BF surfaces along the diagonals of a cube in momentum space.

Both coefficients are positive (as the inset in Fig. 1 shows), and consequently the cyclic state that minimizes both quartic terms is favored below T_c. Remarkably, the coefficient q_3, while finite, is proportional to $\ln(1/t)$, and thus parametrically smaller than q_1 and q_2, which are both proportional to t^{-2}. The RSW semimetals are a rare example of an electronic system where the d-wave superconducting state in the weak-coupling regime is uniquely determined already at the quartic level of the mean-field theory.

B. Nodal structure of the gap

In this section, we study the quasiparticle spectrum for different superconducting states (uniaxial nematic, ferromagnetic, and cyclic state) in the weak-coupling regime and investigate how it changes compared to the strong-coupling regime.

We first show that the energetically preferred cyclic state exhibits BF surfaces. For this we compute the determinant of $H_{\mathrm{BdG}}(\mathbf{p})_{\mathrm{cyclic}}$ defined in Eq. (42) with $\vec{\Delta}_{\mathrm{cyclic}} = \frac{\Delta}{\sqrt{2}}(1, i, 0, 0, 0)$, to find

$$\det\left(H_{\mathrm{BdG}}(\mathbf{p})\right)_{\mathrm{cyclic}} = \mu^4(2\Delta^2 + \mu^2)^2 + \frac{81p^8}{256} + \frac{9}{16}p^6(\Delta^2 - 5\mu^2) + \frac{1}{8}p^4(2\Delta^4 + 29\Delta^2\mu^2 + 59\mu^4)$$

$$- p^2(2\Delta^4\mu^2 + 9\Delta^2\mu^4 + 5\mu^6) + \frac{3}{8}\Delta^2\mu^2p^4[8\sin^4(\theta_{\mathbf{p}})\cos(4\varphi_{\mathbf{p}}) + 4\cos(2\theta_{\mathbf{p}}) + 7\cos(4\theta_{\mathbf{p}})]. \quad (56)$$

The appearance of the BF surfaces from this expression can be understood in the following way. First, it is easy to check that the function of the spherical angles featured in the square brackets in the last line reaches its minimal value (of $-31/3$) along the four diagonal directions $\mathbf{p} \propto (1, 1, 1)$, $(-1, 1, 1)$, $(1, -1, 1)$, and $(1, 1, -1)$. Second, at $\Delta = 0$ the above determinant as a function of p is non-negative, with two local minima at p_1 and p_2, i.e., at the Fermi surfaces of the normal state. At these two minima the determinant vanishes. By taking a derivative with respect to Δ^2 one then readily finds that the determinant must become negative in vicinity of both Fermi momenta p_1 and p_2, at and close to the above diagonal directions, for infinitesimal value of Δ. These intervals of negative determinant then shrink to zero as the direction deviates sufficiently from the diagonal directions.

We therefore find (i) eight BF surfaces in the form of three-dimensional ellipsoids appearing at the first normal state Fermi sphere with $p_1 = 2\mu/3$, and (ii) eight BF surfaces

appearing at the second normal state Fermi sphere with $p_2 = 2\mu$ [see Fig. 5(c)]. A more detailed calculation of the allowed parameter range for the BF surfaces is presented in Appendix D 3. It is interesting to note that the quasiparticle spectrum appears to have the cubic symmetry, which is higher than the tetragonal symmetry of the superconducting order parameter in the cyclic state.

The other prominent state that breaks time-reversal symmetry maximally is the ferromagnetic state. An analysis of the corresponding determinant shows that the ferromagnetic state exhibits four BF surfaces aligned along to the (0,0,1) direction. They are centered at the normal state Fermi surfaces of the normal state and have a bigger diameter than the BF surfaces of the cyclic state [see Fig. 5(b)].

In the case of the real uniaxial nematic state, the state preserves time-reversal symmetry and does not exhibit BF surfaces. Instead, we find four line nodes which constitute two parallel circles on each of the two normal state Fermi surfaces,

hence preserving the remaining SO(2) symmetry. The line nodes occur at momenta p_+ and p_-, respectively, with an inclination $\pm\theta_{\mathbf{p}} = \pm \arccos(\pm 1/\sqrt{3})$. The absolute value of the momentum $\mathbf{p}$ of the four line nodes for $\Delta \ll \mu^2$ reads as $p_- = \frac{2\mu}{3} + \frac{5\Delta^2}{6}$ and $p_+ = 2\mu - \frac{\Delta^2}{2\mu}$. We display the line nodes of the uniaxial nematic state in Fig. 5(a).

IV. CONCLUSIONS

In sum, we studied the *d*-wave superconducting instability of the Rarita-Schwinger-Weyl (RSW) three-dimensional semimetal. A candidate material has recently been proposed in Refs. [16,82]. In the strong-coupling regime with the chemical potential at the Fermi point $\mu = 0$, the computed quartic terms of Ginzburg-Landau free energy for the superconducting *d*-wave (complex tensor) state imply a time-reversal preserving (real tensor) order parameter. The next-order (sextic) terms then predict that the energetically preferred state among the real states is the uniaxial nematic, SO(2)-symmetric state. The uniaxial nematic state has a fully gapped spectrum of the Bogoliubov quasiparticles.

In the weak-coupling regime with finite chemical potential μ, the computed quartic terms imply first that, as typically is the case, maximal breaking of time reversal is energetically preferred. The degeneracy between various time-reversal symmetry-breaking order parameters is now resolved already at the level of quartic terms since we find that the term that is proportional to the state's average magnetization and which is usually missing is now small (compared to the other two terms), but positive. This implies that the *d*-wave state energetically preferred right below the critical temperature is the cyclic state, which breaks the time-reversal symmetry maximally, but at the same time has vanishing average magnetization. Modulo rotation and phase transformation, the cyclic state is unique such a state in the spin-2 Hilbert space of the *d*-wave order parameter. Its experimental manifestation may be the polar Kerr effect, showing the breaking of the time-reversal symmetry, accompanied by the zero magnetization in muon spin resonance, for example.

Even though the RSW Hamiltonian is odd under inversion, the cyclic state exhibits 16 Bogoliubov-Fermi (BF) mini surfaces. We checked several other time-reversal symmetry-breaking states, including the ferromagnetic state, and always found such BF surfaces to be present. We gave an argument why the absence of inversion in the electronic Hamiltonian allows for the appearance of the BF surfaces, by showing that the determinant of the BdG Hamiltonian is not necessarily positive when the time reversal is broken in the superconducting state. We did not prove, however, that BF surfaces must appear in this situation, although we found no example yet of the time-reversal broken state without it. Similar result was found also in a particular time-reversal broken superconducting state in $j = 1$ fermions in Ref. [83]. In contrast to BF surfaces in inversion-symmetric systems, in the systems without inversion symmetry they are here nondegenerate at a fixed momentum at the surface. This makes them immune to the further spontaneous breaking of inversion in presence of favorable interactions recently discussed in Ref. [76]. The BF surfaces should lead to modified power laws in low-temperature magnetic field penetration depth and thermal conductivity, due to a finite, albeit rather small, density of states at zero energy.

APPENDIX A: DIRAC MATRICES

We define the traceless second-rank tensor $S_{ij} = J_i J_j + J_j J_i - \frac{5}{2}\delta_{ij}\mathbb{1}_{4\times 4}$. The five Dirac matrices γ_a can be expressed as a combination of S_{ij} and the real Gell-Mann matrices by

$$\gamma_a = \frac{1}{2\sqrt{3}} S_{ij} M_{ij}^a. \tag{A1}$$

The real Gell-Mann matrices are given by

$$M^1 = \begin{pmatrix} 1 & 0 & 0 \\ 0 & -1 & 0 \\ 0 & 0 & 0 \end{pmatrix}, \quad M^2 = \frac{1}{\sqrt{3}}\begin{pmatrix} -1 & 0 & 0 \\ 0 & -1 & 0 \\ 0 & 0 & 2 \end{pmatrix},$$

$$M^3 = \begin{pmatrix} 0 & 0 & 1 \\ 0 & 0 & 0 \\ 1 & 0 & 0 \end{pmatrix}, \quad M^4 = \begin{pmatrix} 0 & 0 & 0 \\ 0 & 0 & 1 \\ 0 & 1 & 0 \end{pmatrix}, \quad M^5 = \begin{pmatrix} 0 & 1 & 0 \\ 1 & 0 & 0 \\ 0 & 0 & 0 \end{pmatrix}. \tag{A2}$$

For our particular choice of the matrices J_i, the γ matrices are defined as

$$\gamma_1 = \begin{pmatrix} 0 & 0 & 1 & 0 \\ 0 & 0 & 0 & 1 \\ 1 & 0 & 0 & 0 \\ 0 & 1 & 0 & 0 \end{pmatrix}, \quad \gamma_2 = \begin{pmatrix} 1 & 0 & 0 & 0 \\ 0 & -1 & 0 & 0 \\ 0 & 0 & -1 & 0 \\ 0 & 0 & 0 & 1 \end{pmatrix}, \tag{A3a}$$

$$\gamma_3 = \begin{pmatrix} 0 & 1 & 0 & 0 \\ 1 & 0 & 0 & 0 \\ 0 & 0 & 0 & -1 \\ 0 & 0 & -1 & 0 \end{pmatrix}, \quad \gamma_4 = \begin{pmatrix} 0 & -i & 0 & 0 \\ i & 0 & 0 & 0 \\ 0 & 0 & 0 & i \\ 0 & 0 & -i & 0 \end{pmatrix}, \tag{A3b}$$

$$\gamma_5 = \begin{pmatrix} 0 & 0 & -i & 0 \\ 0 & 0 & 0 & -i \\ i & 0 & 0 & 0 \\ 0 & i & 0 & 0 \end{pmatrix}. \tag{A3c}$$

APPENDIX B: SYMMETRY PROPERTIES OF THE QUASIPARTICLE EXCITATION SPECTRUM

In this Appendix we show that for the RSW Hamiltonian $H_0(\mathbf{p}) = \mathbf{p} \cdot \mathbf{J}$, without the inversion symmetry, no operator can introduce the symmetry between positive and negative energies in the superconducting state at fixed momentum, i.e., with the momentum treated simply as a parameter, if time-reversal symmetry is broken, and even at $\mu = 0$. In other words, we show that there is no ($\mathbf{p}$-independent) operator $\mathcal{O}$, linear or antilinear, so that

$$\{H_{\text{BdG}}(\mathbf{p}), \mathcal{O}\} = 0 \tag{B1}$$

with $H_{\text{BdG}}(\mathbf{p})$ from Eq. (43), and the three numbers $\mathbf{p}$ arbitrary.

(i) Let us assume the operator $\mathcal{O}$ first to be linear. Since the three J_i form an irreducible representation of the SO(3) algebra, Schur's lemma implies that the only operator all three generators commute with is proportional to the unit matrix. Since J_i transform as a vector, the only operator that anticommutes with J_1 and J_3 is $\mathcal{U} = e^{i\pi J_2}$, which then evidently commutes with J_2. So, there is no linear operator that anticommutes with all three J_i. This implies that the term $\sigma_3 \otimes H_0$ anticommutes only with $\sigma_1 \otimes \mathbb{1}$ and $\sigma_2 \otimes \mathbb{1}$, which thus are the two possible candidates for $\mathcal{O}$.

The next term of the BdG Hamiltonian $\sigma_1 \otimes \gamma_a$ anticommutes with $\sigma_2 \otimes \mathbb{1}$. So if time reversal is preserved in the superconducting state, i.e., the last term in H_{BdG} is absent, there is a particle-hole symmetry at fixed momentum, and the determinant of the Hamiltonian is non-negative. The last, time-reversal symmetry-breaking term $\sigma_2 \otimes \gamma_b$, however, commutes with $\sigma_2 \otimes \mathbb{1}$. Hence, there is no linear operator that would anticommute with the entire H_{BdG} at fixed momentum, in absence of time-reversal symmetry, even if $\mu = 0$. The same is then true at $\mu \neq 0$.

(ii) Let us next assume that the operator $\mathcal{O}$ is antilinear. For fixed momentum $\mathbf{p}$, we have

$$\{H_0(\mathbf{p}), \mathcal{U}\mathcal{K}\} = 0, \tag{B2}$$

with $\mathcal{U}\mathcal{K}$ being the unique (time-reversal) operator that anticommmutes with all three J_i. Then, $\sigma_3 \otimes H_0$ anticommutes with $\mathbb{1} \otimes \mathcal{U}\mathcal{K}$ and $\sigma_3 \otimes \mathcal{U}\mathcal{K}$:

$$\{\sigma_3 \otimes H_0, \mathbb{1} \otimes \mathcal{U}\mathcal{K}\} = \{\sigma_3 \otimes H_0, \sigma_3 \otimes \mathcal{U}\mathcal{K}\} = 0. \tag{B3}$$

On the other hand, all γ matrices are even under $\mathcal{U}\mathcal{K}$, i.e., $[\gamma_a, \mathcal{U}\mathcal{K}] = 0$. This implies that the second term $\sigma_1 \otimes \gamma_a$ satisfies

$$[\sigma_1 \otimes \gamma_a, \mathbb{1} \otimes \mathcal{U}\mathcal{K}] = 0, \quad \{\sigma_1 \otimes \gamma_a, \sigma_3 \otimes \mathcal{U}\mathcal{K}\} = 0. \tag{B4}$$

However, since σ_2 is imaginary, the last term $\sigma_2 \otimes \gamma_b$ behaves precisely in the opposite way:

$$\{\sigma_2 \otimes \gamma_b, \mathbb{1} \otimes \mathcal{U}\mathcal{K}\} = 0, \quad [\sigma_2 \otimes \gamma_b, \sigma_3 \otimes \mathcal{U}\mathcal{K}] = 0. \tag{B5}$$

So, neither $\mathbb{1} \otimes \mathcal{U}\mathcal{K}$ nor $\sigma_3 \otimes \mathcal{U}\mathcal{K}$ anticommute with $H_{\text{BdG}} = \sigma_3 \otimes H_0 + \Delta_1 \sigma_1 \otimes \gamma_a + \Delta_2 \sigma_2 \otimes \gamma_b$ for $\mathbf{p}$ considered as fixed parameter.

We conclude that in general there is no spectral symmetry between positive and negative energies of $H_{\text{BdG}}(\mathbf{p})$ at a fixed generic momentum $\mathbf{p}$, for systems without inversion symmetry and broken time-reversal symmetry.

APPENDIX C: COEFFICIENTS OF THE FREE-ENERGY EXPANSION

In this Appendix, we give the explicit expressions for the coefficients in the Ginzburg-Landau expansion of the free energy. In the first part, we show the coefficients in the strong-coupling regime with $\mu = 0$. In the second part, we focus on the weak-coupling regime with finite chemical potential μ and demonstrate how the analytic expression of the critical temperature and the analytic expression of the quartic coefficients q_i are derived.
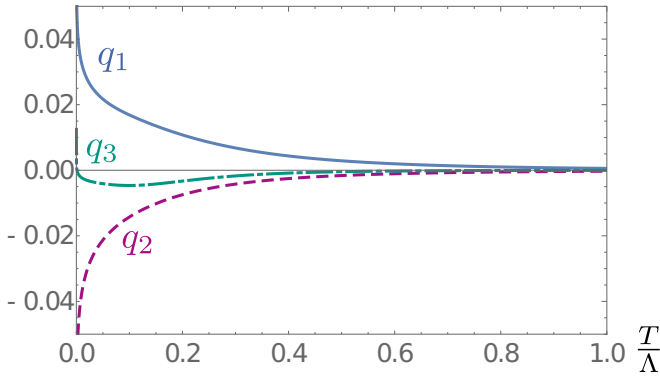
FIG. 6. The quartic coefficients q_i in dependence on the temperature T normalized by the cutoff Λ for $\Lambda = 1$ in the strong-coupling regime. The blue solid line denotes the coefficient q_1, the purple dashed line the coefficient q_2, and the dashed-and-dotted green line the coefficient q_3.

1. Strong-coupling regime

For $\mu = 0$, the coefficient r that is proportional to the quadratic expansion term of the free energy and that is defined

in Eq. (30) is given by

$$
r = \frac{1}{g} - T \sum_n \int_{\mathbf{q}}^{\Lambda} \frac{2}{\omega_n^2 + \frac{9}{4}q^2}
$$
$$
= \frac{1}{g} - \frac{1}{g_c} - \left(T \sum_n \int_{\mathbf{q}}^{\Lambda} \frac{2}{\omega_n^2 + \frac{9}{4}q^2} - \frac{2}{3} \int_{\mathbf{q}}^{\Lambda} \frac{1}{q} \right), \quad \text{(C1)}
$$

where the coupling constant g is positive, $g > 0$, and the "critical coupling" g_c is defined by $g_c = \frac{6\pi^2}{\Lambda^2}$. The numerical values of the coefficients of the quartic terms defined in Eq. (31) are determined by

$$
q_1 = T \sum_n \int_{\mathbf{q}}^{\Lambda} \frac{2\left(\omega_n^4 + \frac{7}{6}\omega_n^2 q^2 - \frac{3}{80}q^4\right)}{\left(\omega_n^2 + \frac{1}{4}q^2\right)^2 \left(\omega_n^2 + \frac{9}{4}q^2\right)^2}, \quad \text{(C2)}
$$

$$
q_2 = -T \sum_n \int_{\mathbf{q}}^{\Lambda} \frac{\omega_n^4 + \frac{11}{6}\omega_n^2 q^2 + \frac{21}{80}q^4}{\left(\omega_n^2 + \frac{1}{4}q^2\right)^2 \left(\omega_n^2 + \frac{9}{4}q^2\right)^2}, \quad \text{(C3)}
$$

$$
q_3 = -T \sum_n \int_{\mathbf{q}}^{\Lambda} \frac{2q^2\left(\omega_n^2 - \frac{3}{20}q^2\right)}{\left(\omega_n^2 + \frac{1}{4}q^2\right)^2 \left(\omega_n^2 + \frac{9}{4}q^2\right)^2}. \quad \text{(C4)}
$$

The numerical value of the coefficients $q_{1,2,3}$ in dependence on the temperature is shown in Fig. 6. We observe that q_1 is always positive, the coefficient q_2 is negative, and the value q_3 is such that a real ground state is selected (see Fig. 1). The sextic terms in the expansion, which eventually lift the degeneracy between the real states, are given by

$$
s_1 = -\frac{1}{840} T \sum_n \int_{\mathbf{q}}^{\Lambda} \frac{2240\omega_n^6 + 6160\omega_n^4 q^2 - 3612\omega_n^2 q^4 + 27q^6}{\left(\omega_n^2 + \frac{1}{4}q^2\right)^3 \left(\omega_n^2 + \frac{9}{4}q^2\right)^3}, \quad \text{(C5)}
$$

$$
s_2 = \frac{1}{3360} T \sum_n \int_{\mathbf{q}}^{\Lambda} \frac{6720\omega_n^6 + 9520\omega_n^4 q^2 - 84\omega_n^2 q^4 + 513q^6}{\left(\omega_n^2 + \frac{1}{4}q^2\right)^3 \left(\omega_n^2 + \frac{9}{4}q^2\right)^3}, \quad \text{(C6)}
$$

$$
s_3 = -\frac{1}{35} T \sum_n \int_{\mathbf{q}}^{\Lambda} \frac{\left(28\omega_n^2 - q^2\right)q^4}{\left(\omega_n^2 + \frac{1}{4}q^2\right)^3 \left(\omega_n^2 + \frac{9}{4}q^2\right)^3}, \quad \text{(C7)}
$$

$$
s_4 = \frac{1}{35} T \sum_n \int_{\mathbf{q}}^{\Lambda} \frac{\left(28\omega_n^2 - 9q^2\right)q^4}{\left(\omega_n^2 + \frac{1}{4}q^2\right)^3 \left(\omega_n^2 + \frac{9}{4}q^2\right)^3}, \quad \text{(C8)}
$$

$$
s_5 = \frac{1}{70} T \sum_n \int_{\mathbf{q}}^{\Lambda} \frac{\left(560\omega_n^4 - 280\omega_n^2 q^2 - 9q^4\right)q^2}{\left(\omega_n^2 + \frac{1}{4}q^2\right)^3 \left(\omega_n^2 + \frac{9}{4}q^2\right)^3}. \quad \text{(C9)}
$$

Note that the integral for $s_3 + s_4$ has a negative-definite integrand. This implies that the uniaxial nematic state is energetically favored among the real order parameters.

2. Weak-coupling regime

For finite chemical potential $\mu \neq 0$, the quadratic coefficient r is given by

$$
r(g, \mu, T, \Lambda) = \frac{1}{g} - \frac{1}{2} K_{11}(T, \mu, \Lambda), \quad \text{(C10)}
$$

where

$$
K_{11} = T \sum_n \int_{\mathbf{q}}^{\Lambda} \frac{8\left(128(\mu^2 + \omega^2)^3 + 18q^6 + \frac{8}{5}q^4(59\mu^2 + 95\omega^2) - 32q^2(9\mu^4 - 2\mu^2\omega^2 - 11\omega^4)\right)}{[q^2 - 4(\mu - i\omega)^2][9q^2 - 4(\mu - i\omega)^2][q^2 - 4(\mu + i\omega)^2][9q^2 - 4(\mu + i\omega)^2]}. \quad \text{(C11)}
$$

The Matsubara summation and momentum integration can be performed numerically. We can analytically approximate the integrand after Matsubara summation by expanding the integrand around the divergences at $q = \frac{2}{3}$ and $q = 2$. For small t we

have

$$K_{11} \approx \int_{\kappa_0}^{\kappa_1} dq \, \mathrm{int}_{2/3}(q) + \int_{\kappa_1}^{\kappa_2} dq \, \mathrm{int}_2(q) + \int_{\kappa_2}^{\Lambda} dq \, \mathrm{int}_{\infty}(q)$$

$$= \frac{2}{g_c} + \int_{\kappa_0}^{\kappa_1} dq \, \mathrm{int}_{2/3}(q) + \int_{\kappa_1}^{\kappa_2} dq \, \mathrm{int}_2(q) - \int_0^{\kappa_2} dq \, \mathrm{int}_{\infty}(q) \tag{C12}$$

with the leading singular contributions for $t = T/\mu \to 0$ to the integrand around $q \approx \frac{2}{3}$, 2, ∞ given by

$$\mathrm{int}_{2/3}(q) = \frac{\mu}{\frac{135}{2}\pi^2 |q/\mu - \frac{2}{3}| + 90\pi^2 t}, \tag{C13}$$

$$\mathrm{int}_2(q) = \frac{\mu}{\frac{5}{2}\pi^2 |q/\mu - 2| + 10\pi^2 t}, \tag{C14}$$

$$\mathrm{int}_{\infty}(q) = \frac{q}{\frac{3}{2}\pi^2}. \tag{C15}$$

We then find

$$K_{11} \approx \frac{2}{g_c} - \frac{\kappa_2^2}{3\pi^2} + \frac{2\mu^2}{135\pi^2}\left[\ln\left(1 + \frac{2 - 3\frac{\kappa_0}{\mu}}{4t}\right) + \ln\left(1 + \frac{3\frac{\kappa_1}{\mu} - 2}{4t}\right)\right] + \frac{2\mu^2}{5\pi^2}\left[\ln\left(1 + \frac{2 - \frac{\kappa_1}{\mu}}{4t}\right) + \ln\left(1 + \frac{\frac{\kappa_2}{\mu} - 2}{4t}\right)\right]$$

$$= -\frac{112\mu^2}{135\pi^2}\ln t + \frac{2}{g_c} - \frac{a}{3\pi^2}\mu^2, \tag{C16}$$

where the divergent term $\propto \ln t$ is universal and independent of the approximations made to the finite part of the integral. In contrast, the t-independent term a is nonuniversal. We fix a by comparing the right-hand side to the numerically evaluated K_{11} to be $a = 0.613$. This leads to

$$r(g, \mu, T, \Lambda) \simeq \frac{1}{g} - \frac{1}{g_c} + \frac{a}{6\pi^2}\mu^2 + \frac{56\mu^2}{135\pi^2}\ln t \tag{C17}$$

and from $r(g, \mu, T_c, \Lambda) = 0$ we deduce

$$\frac{T_c}{\mu} \simeq \exp\left[-\frac{135\pi^2}{56\mu^2 g_c}\left(\frac{g_c}{g} - 1 + \frac{a}{6\pi^2}g_c\mu^2\right)\right] = \exp\left[-\frac{45}{112}\frac{\Lambda^2}{\mu^2}\left(\frac{g_c}{g} - 1 + a\frac{\mu^2}{\Lambda^2}\right)\right] \tag{C18}$$

as quoted in Eq. (52).

The quartic coefficients for finite μ are given by

$$q_1(T, \mu) = -T\sum_n \int_\mathbf{q}^\Lambda \frac{32}{105[q^2 - 4(\mu - i\omega)^2]^2[9q^2 - 4(\mu - i\omega)^2]^2[q^2 - 4(\mu + i\omega)^2]^2[9q^2 - 4(\mu + i\omega)^2]^2}$$

$$\times [-430080(\mu^2 + \omega^2)^6 + 5103q^{12} - 648q^{10}(373\mu^2 + 175\omega^2) - 48q^8(4189\mu^4 + 72906\mu^2\omega^2 + 29757\omega^4)$$

$$+ 256q^6(6949\mu^6 + 39889\mu^4\omega^2 - 13141\mu^2\omega^4 - 18865\omega^6)$$

$$- 1792q^4(\mu^2 + \omega^2)^2(1529\mu^4 - 3902\mu^2\omega^2 + 3161\omega^4) + 71680q^2(\mu^2 + \omega^2)^4(25\mu^2 - 37\omega^2)], \tag{C19}$$

$$q_2(T, \mu) = -T\sum_n \int_\mathbf{q}^\Lambda \frac{16}{105[q^2 - 4(\mu - i\omega)^2]^2[9q^2 - 4(\mu - i\omega)^2]^2[q^2 - 4(\mu + i\omega)^2]^2[9q^2 - 4(\mu + i\omega)^2]^2}$$

$$\times [430080(\mu^2 + \omega^2)^6 + 35721q^{12} - 648q^{10}(967\mu^2 - 875\omega^2) + 48q^8(30317\mu^4 - 10518\mu^2\omega^2 + 66381\omega^4)$$

$$- 256q^6(7169\mu^6 - 3571\mu^4\omega^2 - 24401\mu^2\omega^4 - 29645\omega^6)$$

$$+ 1792q^4(\mu^2 + \omega^2)^2(1633\mu^4 - 2542\mu^2\omega^2 + 4033\omega^4) - 71680q^2(29\mu^2 - 41\omega^2)(\mu^2 + \omega^2)^4], \tag{C20}$$

$$q_3(T, \mu) = +T\sum_n \int_\mathbf{q}^\Lambda \frac{128\,q^2}{35[q^2 - 4(\mu - i\omega)^2]^2[9q^2 - 4(\mu - i\omega)^2]^2[q^2 - 4(\mu + i\omega)^2]^2[9q^2 - 4(\mu + i\omega)^2]^2}$$

$$\times [35840(\mu^2 - \omega^2)(\mu^2 + \omega^2)^4 + 1701q^{10} + 108q^8(93\mu^2 + 35\omega^2) - 96q^6(1277\mu^4 + 1418\mu^2\omega^2 + 637\omega^4)$$

$$+ 128q^4(2047\mu^6 + 4327\mu^4\omega^2 + 857\mu^2\omega^4 - 1855\omega^6) - 1792q^2(\mu^2 + \omega^2)^2(97\mu^4 + 50\mu^2\omega^2 + 97\omega^4)]. \tag{C21}$$

The integrals are convergent and readily evaluated numerically. In order to find an analytical expression, we first introduce dimensionless variables with $k = q/\mu$ and $t = T/\mu$. Then, we perform a zero-temperature frequency integration and then expand around $k = \frac{2}{3}$ and 2. This way, we can determine the divergence of the integrand, i.e., whether the integrand is proportional to

$1/k^3$, $1/k^2$, or $1/k$. Next, we perform the Matsubara summation for the original expressions in Eqs. (C19), (C20), and (C21) and expand them around $k = \frac{2}{3}$ and 2, in order to extract the temperature dependence of the integrand at these singular points. With this knowledge, we can make an appropriate approximate ansatz for the integrands of $q_{1,2,3}$ and establish the analytic divergence structure of the coefficients. The integrand of q_1 is described by

$$\mathrm{int}_{q_1}(\mathrm{k} \approx 2/3) = \frac{1}{8505\pi^2|k - \frac{2}{3}|^3/2 + 15120\pi^2 t^3}\left[1 - \frac{45}{4}\left(k - \frac{2}{3}\right) - \frac{117}{4}\left(k - \frac{2}{3}\right)^2\right], \tag{C22}$$

$$\mathrm{int}_{q_1}(\mathrm{k} \approx 2) = \frac{1}{35\pi^2|k - 2|^3/2 + 1680\pi^2 t^3}\left[1 + \frac{3}{4}(k - 2)\right], \tag{C23}$$

$$\mathrm{int}_{q_1}(\mathrm{k} \approx \infty) = \frac{1}{15\pi^2 k}. \tag{C24}$$

For the integrand of q_2 we find

$$\mathrm{int}_{q_2}\left(\mathrm{k} \approx \frac{2}{3}\right) = \frac{1}{8505\pi^2\left|k - \frac{2}{3}\right|^3 + 30240\pi^2 t^3}\left[1 + 9\left(k - \frac{2}{3}\right) - \frac{261}{2}\left(k - \frac{2}{3}\right)^2\right], \tag{C25}$$

$$\mathrm{int}_{q_2}(\mathrm{k} \approx 2) = \frac{1}{35\pi^2|k - 2|^3 + 3360\pi^2 t^3}\left[1 + (k - 2) - \frac{3}{2}(k - 2)^2\right], \tag{C26}$$

$$\mathrm{int}_{q_2}(\mathrm{k} \approx \infty) = -\frac{1}{10\pi^2 k}. \tag{C27}$$

At last, the coefficient q_3 is given by the functions

$$\mathrm{int}_{q_3}(\mathrm{k} \approx 2/3) = \frac{-1}{1890\pi^2\left[\left(k - \frac{2}{3}\right)^2 + 2t^2\right]}\frac{k - \frac{2}{3}}{\sqrt{\left(k - \frac{2}{3}\right)^2 + 2t^2}} + \frac{2}{315\pi^2\left[\sqrt{\left(k - \frac{2}{3}\right)^2 + t}\right]}, \tag{C28}$$

$$\mathrm{int}_{q_3}(\mathrm{k} \approx 2) = \frac{3}{70\pi^2[(k - 2)^2 + 18t^2]}\frac{k - 2}{\sqrt{(k - 2)^2 + 18t^2}} + \frac{3}{70\pi^2[\sqrt{(k - 2)^2 + t}]}, \tag{C29}$$

$$\mathrm{int}_{q_3}(\mathrm{k} \approx \infty) = \frac{1}{90\,k\pi^2}. \tag{C30}$$

After performing the momentum integration in Eqs. (C22)–(C30) with these approximations, and fitting the nondivergent part to match the full expression as in Eq. (C16), we obtain the analytic expressions for the coefficients $q_{1,2,3}$ given in Eqs. (53), (54), and (55).

APPENDIX D: NODAL STRUCTURE OF THE SUPERCONDUCTING GAP

In this Appendix, we derive the nodal structure of the superconducting gap in the weak-coupling limit for $\mu \neq 0$ for the three relevant superconducting orders due to Fig. 1: the real uniaxial nematic state, and the time-reversal symmetry-breaking ferromagnetic and cyclic state. While the former case exhibits four circular line nodes, the latter two states feature BF surfaces.

1. Uniaxial nematic state

The determinant of the uniaxial state with $\vec{\Delta}_{\mathrm{uniaxial}} = \Delta(0, 1, 0, 0, 0)$ is

$$\det\left(H_{\mathrm{BdG}}(\mathbf{p})\right)_{\mathrm{uniaxial}} = \left(\frac{9}{16}\right)^2\left[p^4 + (A + B)p^2 + \frac{16}{9}(\Delta^2 + \mu^2)^2\right]\left[p^4 + (A - B)p^2 + \frac{16}{9}(\Delta^2 + \mu^2)^2\right] \tag{D1}$$

with

$$A = \frac{8}{9}[2\Delta^2 - 5\mu^2 + 3\Delta^2\cos(2\theta_\mathbf{p})], \tag{D2}$$

$$B = \frac{8}{9}\sqrt{2}i\Delta\mu\sqrt{11 + 12\cos(2\theta_\mathbf{p}) + 9\cos(4\theta_\mathbf{p})}. \tag{D3}$$

Any zero p of the determinant must satisfy

$$p^2 = -\frac{A + B}{2} \pm \frac{1}{2}\sqrt{(A + B)^2 - \frac{64}{9}(\Delta^2 + \mu^2)^2}. \tag{D4}$$

In order for p^2 to be real, $B = 0$, which yields $\theta_\mathbf{p} \equiv \theta_0$ with

$$11 + 12\cos(2\theta_0) + 9\cos(4\theta_0) = 0 \Leftrightarrow \theta_0 = \arccos\left(\pm\frac{1}{\sqrt{3}}\right). \tag{D5}$$

This leads to the condition

$$p^2 = \frac{4}{9}(-\Delta^2 + 5\mu^2 \pm 2\sqrt{-2\Delta^4 - 7\Delta^2\mu^2 + 4\mu^4}). \tag{D6}$$

Hence, we have four nodal loops for the uniaxial state located at

$$(p_\pm, \theta_0), \quad (p_\pm, -\theta_0) \tag{D7}$$

for every $\phi \in [0, 2\pi)$. For $\Delta \ll \mu$ we expand Eq. (D6), and obtain $p_+ = 2\mu - \frac{\Delta^2}{2\mu}$, $p_- = \frac{2\mu}{3} + \frac{5\Delta^2}{6}$.

2. Ferromagnetic state

The determinant for the ferromagnetic state with $\vec{\Delta}_{\text{ferromagnetic}} = \frac{\Delta}{\sqrt{2}}(1, 0, 0, 0, i)$ is

$$\det(H_{\text{BdG}}(\mathbf{p}))_{\text{ferromagnetic}} = \mu^4(2\Delta^2 + \mu^2)^2 + \frac{81p^8}{256} - \frac{45\mu^2 p^6}{16} + \frac{1}{8}p^4(9\Delta^4 + 36\Delta^2\mu^2 + 59\mu^4) - p^2(8\Delta^4\mu^2 + 10\Delta^2\mu^4 + 5\mu^6)$$

$$+ \frac{1}{16}\Delta^2 p^2(6p^2(3\Delta^2 + 2\mu^2)\cos(4\theta_\mathbf{p}) - \cos(2\theta_\mathbf{p})[48\mu^4 + 27p^4 + 8\mu^2(4\Delta^2 - 9p^2)]). \tag{D8}$$

The BF surface derived from the above determinant emerges at $\varphi_\mathbf{p} \in [0, 2\pi)$ and the following value for $\theta_\mathbf{p}$:

$$\begin{aligned}
\theta_{\mathbf{p},\text{ferro}} = \frac{1}{2}\arctan\Bigg[&\frac{1}{\Delta^2 p^4(3\Delta^2 + 2\mu^2)}(27\Delta^2 p^6 - 72\Delta^2\mu^2 p^4 + 16p^2(2\Delta^4\mu^2 + 3\Delta^2\mu^4) \\
&- \sqrt{2}[\Delta^2(-p^4)(9\mu^2 p^2 - 4\mu^4)(-64(16\Delta^6 + 24\Delta^4\mu^2 + 12\Delta^2\mu^4 + 3\mu^6) + 27p^6 - 12p^4(12\Delta^2 + 19\mu^2) \\
&+ 48p^2(8\Delta^4 + 16\Delta^2\mu^2 + 11\mu^4))]^{1/2}), \; -\frac{1}{\sqrt{\Delta^2(-p^4)(3\Delta^2 + 2\mu^2)}}\Bigg(\Bigg[\frac{1}{p^2(3\Delta^2 + 2\mu^2)}(243p^{10}(3\Delta^2 - 2\mu^2) \\
&- 432p^8(3\Delta^2\mu^2 - 10\mu^4) - 96p^6(54\Delta^6 + 126\Delta^4\mu^2 + 99\Delta^2\mu^4 + 118\mu^6) - 32\sqrt{2}\mu^2(2\Delta^2 + 3\mu^2) \\
&\times [\Delta^2(-p^4)(4\mu^4 - 9\mu^2 p^2)(64(16\Delta^6 + 24\Delta^4\mu^2 + 12\Delta^2\mu^4 + 3\mu^6) - 27p^6 + 12p^4(12\Delta^2 + 19\mu^2) \\
&- 48p^2(8\Delta^4 + 16\Delta^2\mu^2 + 11\mu^4))]^{1/2} + 6p^4(3072\Delta^6\mu^2 + 4352\Delta^4\mu^4 + 2176\Delta^2\mu^6 + 1280\mu^8 \\
&- 9\sqrt{2}[\Delta^2(-p^4)(4\mu^4 - 9\mu^2 p^2)(64(16\Delta^6 + 24\Delta^4\mu^2 + 12\Delta^2\mu^4 + 3\mu^6) - 27p^6 + 12p^4(12\Delta^2 + 19\mu^2) \\
&- 48p^2(8\Delta^4 + 16\Delta^2\mu^2 + 11\mu^4))]^{1/2}) - 16\mu^2 p^2(448\Delta^6\mu^2 + 576\Delta^4\mu^4 + 240\Delta^2\mu^6 + 96\mu^8 \\
&- 9\sqrt{2}[\Delta^2(-p^4)(4\mu^4 - 9\mu^2 p^2)(64(16\Delta^6 + 24\Delta^4\mu^2 + 12\Delta^2\mu^4 + 3\mu^6) - 27p^6 + 12p^4(12\Delta^2 + 19\mu^2) \\
&- 48p^2(8\Delta^4 + 16\Delta^2\mu^2 + 11\mu^4))]^{1/2}))\Bigg]^{1/2}\Bigg)\Bigg] + \pi c_1, \tag{D9}
\end{aligned}$$

where $\arctan[x, y]$ denotes the inverse tangent of y/x taking into account which quadrant the point (x, y) is located and $c_1 \in \mathbb{Z}$. The angle $\theta_{\mathbf{p},\text{ferro}}$ is real valued if the absolute value of the momentum p is within the following intervals, for small Δ:

$$\frac{2\mu}{3} \leqslant p \leqslant \frac{2\mu}{3} + \frac{\Delta^2}{\mu}, \tag{D10}$$

$$2\mu \leqslant p \leqslant 2\mu + \frac{\Delta^2}{\mu}. \tag{D11}$$

These are then the extents of the two BF surfaces along (0,0,1) direction. As the angle $\theta_\mathbf{p}$ is increased from zero (or decreased from π) the two intervals eventually shrink to zero, meanwhile producing a BF surface.

3. Cyclic state

The determinant of the cyclic state is given by

$$\det(H_{\text{BdG}}(\mathbf{p}))_{\text{cyclic}} = \mu^4(2\Delta^2 + \mu^2)^2 + \frac{81p^8}{256} + \frac{9}{16}p^6(\Delta^2 - 5\mu^2) + \frac{1}{8}p^4(2\Delta^4 + 29\Delta^2\mu^2 + 59\mu^4)$$

$$- p^2(2\Delta^4\mu^2 + 9\Delta^2\mu^4 + 5\mu^6) + \frac{3}{8}\Delta^2\mu^2 p^4(8\sin^4(\theta_\mathbf{p})\cos(4\varphi_\mathbf{p}) + 4\cos(2\theta_\mathbf{p}) + 7\cos(4\theta_\mathbf{p})). \tag{D12}$$

In order to find the zeros of the determinant, we first write $\det(H_{\text{BdG}}(\mathbf{p}))_{\text{cyclic}} = 0$ as

$$8\sin^4(\theta_\mathbf{p})\cos(4\varphi_\mathbf{p}) + 4\cos(2\theta_\mathbf{p}) + 7\cos(4\theta_\mathbf{p}) = -R(p, \mu, \Delta) \tag{D13}$$

with

$$R(p, \mu, \Delta) = \frac{59\mu^2}{3\Delta^2} + \frac{2\Delta^2}{3\mu^2} + \frac{8\mu^6}{3\Delta^2 p^4} + \frac{32\Delta^2\mu^2}{3p^4} + \frac{27p^4}{32\Delta^2\mu^2} + \frac{32\mu^4}{3p^4}$$
$$ - \frac{40\mu^4}{3\Delta^2 p^2} - \frac{16\Delta^2}{3p^2} - \frac{15p^2}{2\Delta^2} - \frac{24\mu^2}{p^2} + \frac{3p^2}{2\mu^2} + \frac{29}{3}. \tag{D14}$$

We can solve the above equation for $\varphi_{\mathbf{p}}$ and find

$$\varphi_{\mathbf{p}} = \pm\frac{1}{4}\left[\arccos\left(-\frac{1}{8\sin^4(\theta_{\mathbf{p}})}[R(p,\mu,\Delta) + 4\cos(2\theta_{\mathbf{p}}) + 7\cos(4\theta_{\mathbf{p}})]\right) + 2\pi\right]. \tag{D15}$$

This expression implies restrictions on the parameters R, p, $\theta_{\mathbf{p}}$ since the argument x of the inverse cosine function has to be in the interval $-1 \leqslant x \leqslant 1$. This sets the following limits on the variable $\theta_{\mathbf{p}}$:

$$\arctan(\sqrt{4 - \sqrt{31 - 3R}}, \sqrt{8 - \sqrt{31 - 3R}}) \leqslant \theta_{\mathbf{p},1} \leqslant \arctan(\sqrt{4 - \sqrt{31 - 3R}}, \sqrt{\sqrt{31 - 3R} + 8}), \tag{D16}$$

$$\arctan(-\sqrt{4 - \sqrt{31 - 3R}}, \sqrt{\sqrt{31 - 3R} + 8}) \leqslant \theta_{\mathbf{p},2} \leqslant \arctan(-\sqrt{4 - \sqrt{31 - 3R}}, \sqrt{8 - \sqrt{31 - R}}), \tag{D17}$$

$$\arctan(-\sqrt{\sqrt{31 - 3R} + 4}, -\sqrt{8 - \sqrt{31 - 3R}}) \leqslant \theta_{\mathbf{p},3} \leqslant \arctan(-\sqrt{4 - \sqrt{31 - 3R}}, -\sqrt{\sqrt{31 - 3R} + 8}), \tag{D18}$$

$$\arctan(\sqrt{4 - \sqrt{31 - 3R}}, -\sqrt{\sqrt{31 - 3R} + 8}) \leqslant \theta_{\mathbf{p},4} \leqslant \arctan(\sqrt{\sqrt{31 - 3R} + 4}, -\sqrt{8 - \sqrt{31 - 3R}}). \tag{D19}$$

[Here, $\phi = \arctan(x, y)$ is the artcan of y/x such that $x = \cos\phi$ and $y = \sin\phi$.] These equations, on the other hand, yield further constraints since the square root under the square root has to be real. Hence, the function $R(p, \mu, \Delta)$ has to be in the interval

$$5 \leqslant R(p, \mu, \Delta) \leqslant \frac{31}{3}. \tag{D20}$$

Furthermore, for $\mu \gg \Delta$, also $R > 5$. Solving the equation $R = 31/3$, which corresponds to the four diagonal directions $(1,1,1)$, $(-1, 1, 1)$, $(1, -1, 1)$, and $(1, 1, -1)$, and Taylor expanding the result for small Δ, we find

$$\frac{2\mu}{3} + \frac{\Delta^2}{3\mu} \leqslant p_1 \leqslant \frac{2\mu}{3} + \frac{4\Delta^2}{3\mu}, \tag{D21}$$

$$2\mu - \frac{\Delta^2}{\mu} \leqslant p_2 \leqslant 2\mu. \tag{D22}$$

The nontrivial angular dependence of the BF surfaces that develops as the direction changes from the diagonals in the cyclic state is shown in Fig. 5.

---

[1] A. K. Geim and K. S. Novoselov, The rise of graphene, Nat. Mater. **6**, 183 (2007).

[2] M. Z. Hasan and C. L. Kane, Colloquium: Topological insulators, Rev. Mod. Phys. **82**, 3045 (2010).

[3] H. Gao, J. W. F. Venderbos, Y. Kim, and A. M. Rappe, Topological Semimetals from First Principles, Annu. Rev. Mater. Res. **49**, 153 (2019).

[4] X.-L. Qi and S.-C. Zhang, Topological insulators and superconductors, Rev. Mod. Phys. **83**, 1057 (2011).

[5] E.-G. Moon, C. Xu, Y. B. Kim, and L. Balents, Non-Fermi-Liquid and Topological States with Strong Spin-Orbit Coupling, Phys. Rev. Lett. **111**, 206401 (2013).

[6] I. F. Herbut and L. Janssen, Topological Mott Insulator in Three-Dimensional Systems with Quadratic Band Touching, Phys. Rev. Lett. **113**, 106401 (2014).

[7] T. Kondo, M. Nakayama, R. Chen, J. J. Ishikawa, E.-G. Moon, T. Yamamoto, Y. Ota, W. Malaeb, H. Kanai, Y. Nakashima, Y. Ishida, R. Yoshida, H. Yamamoto, M. Matsunami, S. Kimura, N. Inami, K. Ono, H. Kumigashira, S. Nakatsuji, L. Balents, and S. Shin, Quadratic Fermi node in a 3D strongly correlated semimetal, Nat. Commun. **6**, 10042 (2015).

[8] M. Nakayama, T. Kondo, Z. Tian, J. J. Ishikawa, M. Halim, C. Bareille, W. Malaeb, K. Kuroda, T. Tomita, S. Ideta, K. Tanaka, M. Matsunami, S. Kimura, N. Inami, K. Ono, H. Kumigashira, L. Balents, S. Nakatsuji, and S. Shin, Slater to Mott Crossover in the Metal to Insulator Transition of $Nd_2Ir_2O_7$, Phys. Rev. Lett. **117**, 056403 (2016).

[9] B. Bradlyn, J. Cano, Z. Wang, M. G. Vergniory, C. Felser, R. J. Cava, and B. A. Bernevig, Beyond Dirac and Weyl fermions: Unconventional quasiparticles in conventional crystals, Science **353** (2016).

[10] P. Tang, Q. Zhou, and S.-C. Zhang, Multiple Types of Topological Fermions in Transition Metal Silicides, Phys. Rev. Lett. **119**, 206402 (2017).

[11] G. Chang, B. J. Wieder, F. Schindler, D. S. Sanchez, I. Belopolski, S.-M. Huang, B. Singh, D. Wu, T.-R. Chang, T. Neupert, S.-Y. Xu, H. Lin, and M. Z. Hasan, Topological quantum properties of chiral crystals, Nat. Mater. **17**, 978 (2018).

[12] D. Takane, Z. Wang, S. Souma, K. Nakayama, T. Nakamura, H. Oinuma, Y. Nakata, H. Iwasawa, C. Cacho, T. Kim, K. Horiba, H. Kumigashira, T. Takahashi, Y. Ando, and T. Sato, Observation of Chiral Fermions with a Large Topological Charge and Associated Fermi-Arc Surface States in CoSi, Phys. Rev. Lett. **122**, 076402 (2019).

[13] Z. Rao, H. Li, T. Zhang, S. Tian, C. Li, B. Fu, C. Tang, L. Wang, Z. Li, W. Fan, J. Li, Y. Huang, Z. Liu, Y. Long, C. Fang, H. Weng, Y. Shi, H. Lei, Y. Sun, T. W. Qian, and H. Ding, Observation of unconventional chiral fermions with long Fermi arcs in CoSi, Nature (London) **567**, 496 (2019).

[14] D. S. Sanchez, I. Belopolski, T. A. Cochran, X. Xu, J.-X. Yin, G. Chang, W. Xie, K. Manna, V. Süss, C.-Y. Huang, N. Alidoust, D. Multer, S. S. Zhang, N. Shumiya, X. Wang, G.-Q. Wang, T.-R. Chang, C. Felser, S.-Y. Xu, S. Jia *et al.*, Topological chiral crystals with helicoid-arc quantum states, Nature (London) **567**, 500 (2019).

[15] N. B. M. Schröter, D. Pei, M. G. Vergniory, Y. Sun, K. Manna, F. de Juan, J. A. Krieger, V. Süss, M. Schmidt, P. Dudin, B. Bradlyn, T. K. Kim, C. Cacho, C. Felser, V. N. Strocov, and Y. Chen, Chiral topological semimetal with multifold band crossings and long Fermi arcs, Nat. Phys. **15**, 759 (2019).

[16] B. Q. Lv, Z.-L. Feng, J.-Z. Zhao, Noah F. Q. Yuan, A. Zong, K. F. Luo, R. Yu, Y.-B. Huang, V. N. Strocov, A. Chikina, A. A. Soluyanov, N. Gedik, Y.-G. Shi, T. Qian, and H. Ding, Observation of multiple types of topological fermions in PdBiSe, Phys. Rev. B **99**, 241104(R) (2019).

[17] J. Cano, B. Bradlyn, and M. G. Vergniory, Multifold nodal points in magnetic materials, APL Mater. **7**, 101125 (2019).

[18] W. Rarita and J. Schwinger, On a theory of particles with half-integral spin, Phys. Rev. **60**, 61 (1941).

[19] L. Liang and Y. Yu, Semimetal with both Rarita-Schwinger-Weyl and Weyl excitations, Phys. Rev. B **93**, 045113 (2016).

[20] M. Ezawa, Pseudospin-$\frac{3}{2}$ fermions, type-II Weyl semimetals, and critical Weyl semimetals in tricolor cubic lattices, Phys. Rev. B **94**, 195205 (2016).

[21] Igor Boettcher, Interplay of Topology and Electron-Electron Interactions in Rarita-Schwinger-Weyl Semimetals, Phys. Rev. Lett. **124**, 127602 (2020).

[22] D. Z. Freedman, P. van Nieuwenhuizen, and S. Ferrara, Progress toward a theory of supergravity, Phys. Rev. D **13**, 3214 (1976).

[23] J. M. Luttinger, Quantum theory of cyclotron resonance in semiconductors: General theory, Phys. Rev. **102**, 1030 (1956).

[24] A. A. Abrikosov, Calculation of critical indices fo zero-gap semiconductors, Zh. Eksp. Teor. Fiz. **66**, 1443 (1974) [Sov. Phys.–JETP **39**, 709 (1974)].

[25] A. A. Abrikosov and S. D. Beneslavskii, Possible existence of substances intermediate between metals and dielectrics, Zh. Eksp. Teor. Fiz. **59**, 1280 (1970) [Sov. Phys.–JETP **32**, 699 (1971)].

[26] L. Janssen and I. F. Herbut, Nematic quantum criticality in three-dimensional Fermi system with quadratic band touching, Phys. Rev. B **92**, 045117 (2015).

[27] L. Janssen and I. F. Herbut, Excitonic instability of three-dimensional gapless semiconductors: Large-*N* theory, Phys. Rev. B **93**, 165109 (2016).

[28] L. Janssen and I. F. Herbut, Phase diagram of electronic systems with quadratic Fermi nodes in $2 < d < 4$: $2 + \epsilon$ expansion, $4 - \epsilon$ expansion, and functional renormalization group, Phys. Rev. B **95**, 075101 (2017).

[29] I. Mandal and R. M. Nandkishore, Interplay of Coulomb interactions and disorder in three-dimensional quadratic band crossings without time-reversal symmetry and with unequal masses for conduction and valence bands, Phys. Rev. B **97**, 125121 (2018).

[30] N. P. Butch, P. Syers, K. Kirshenbaum, A. P. Hope, and J. Paglione, Superconductivity in the topological semimetal YPtBi, Phys. Rev. B **84**, 220504(R) (2011).

[31] T. V. Bay, M. Jackson, C. Paulsen, C. Baines, A. Amato, T. Orvis, M. C. Aronson, Y. K. Huang, and A. de Visser, Low field magnetic response of the non-centrosymmetric superconductor YPtBi, Solid State Commun. **183**, 13 (2014).

[32] I. Boettcher and I. F. Herbut, Superconducting quantum criticality in three-dimensional Luttinger semimetals, Phys. Rev. B **93**, 205138 (2016).

[33] M. Meinert, Unconventional Superconductivity in YPtBi and Related Topological Semimetals, Phys. Rev. Lett. **116**, 137001 (2016).

[34] P. M. R. Brydon, L. Wang, M. Weinert, and D. F. Agterberg, Pairing of $j = 3/2$ Fermions in Half-Heusler Superconductors, Phys. Rev. Lett. **116**, 177001 (2016).

[35] M. Smidman, M. B. Salamon, H. Q. Yuan, and D. F. Agterberg, Superconductivity and spin–orbit coupling in non-centrosymmetric materials: a review, Rep. Prog. Phys. **80**, 036501 (2017).

[36] D. F. Agterberg, P. M. R. Brydon, and C. Timm, Bogoliubov Fermi Surfaces in Superconductors with Broken Time-Reversal Symmetry, Phys. Rev. Lett. **118**, 127001 (2017).

[37] S. A. A. Ghorashi, S. Davis, and M. S. Foster, Disorder-enhanced topological protection and universal quantum criticality in a spin-$\frac{3}{2}$ topological superconductor, Phys. Rev. B **95**, 144503 (2017).

[38] W. Yang, T. Xiang, and C. Wu, Majorana surface modes of nodal topological pairings in spin-$\frac{3}{2}$ semimetals, Phys. Rev. B **96**, 144514 (2017).

[39] L. Savary, J. Ruhman, J. W. F. Venderbos, L. Fu, and P. A. Lee, Superconductivity in three-dimensional spin-orbit coupled semimetals, Phys. Rev. B **96**, 214514 (2017).

[40] I. Boettcher and I. F. Herbut, Unconventional Superconductivity in Luttinger Semimetals: Theory of Complex Tensor Order and the Emergence of the Uniaxial Nematic State, Phys. Rev. Lett. **120**, 057002 (2018).

[41] I. Mandal, Fate of superconductivity in three-dimensional disordered Luttinger semimetals, Ann. Phys. **392**, 179 (2018).

[42] J. W. F. Venderbos, L. Savary, J. Ruhman, P. A. Lee, and L. Fu, Pairing States of Spin-$\frac{3}{2}$ Fermions: Symmetry-Enforced Topological Gap Functions, Phys. Rev. X **8**, 011029 (2018).

[43] I. Boettcher and I. F. Herbut, Critical phenomena at the complex tensor ordering phase transition, Phys. Rev. B **97**, 064504 (2018).

[44] H. Kim, K. Wang, Y. Nakajima, R. Hu, S. Ziemak, P. Syers, L. Wang, H. Hodovanets, J. D. Denlinger, P. M. R. Brydon, D. F. Agterberg, M. A. Tanatar, R. Prozorov, and J. Paglione, Beyond triplet: Unconventional superconductivity in a spin-3/2 topological semimetal, Sci. Adv. **4**, eaao4513 (2018).

[45] G. B. Sim, A. Mishra, M. J. Park, Y. B. Kim, G. Y. Cho, and S. B. Lee, Topological $d + s$ wave superconductors in a multiorbital quadratic band touching system, Phys. Rev. B **100**, 064509 (2019).

[46] J. Yu and C.-X. Liu, Singlet-quintet mixing in spin-orbit coupled superconductors with $j = \frac{3}{2}$ fermions, Phys. Rev. B **98**, 104514 (2018).

[47] A. L. Szabó, R. Moessner, and B. Roy, Strain-engineered higher-order topological phases for spin-$\frac{3}{2}$ Luttinger fermions, Phys. Rev. B **101**, 121301(R) (2020).

[48] B. Roy, S. A. A. Ghorashi, M. S. Foster, and A. H. Nevidomskyy, Topological superconductivity of spin-3/2 carriers in a three-dimensional doped Luttinger semimetal, Phys. Rev. B **99**, 054505 (2019).

[49] W. Witczak-Krempa and Y. B. Kim, Topological and magnetic phases of interacting electrons in the pyrochlore iridates, Phys. Rev. B **85**, 045124 (2012).

[50] W. Witczak-Krempa, G. Chen, Y. B. Kim, and L Balents, Correlated quantum phenomena in the strong spin-orbit regime, Annu. Rev. Condens. Matter Phys. **5**, 57 (2014).

[51] L. Savary, E.-G. Moon, and L. Balents, New Type of Quantum Criticality in the Pyrochlore Iridates, Phys. Rev. X **4**, 041027 (2014).

[52] T. Liang, T. H. Hsieh, J. J. Ishikawa, S. Nakatsuji, L. Fu, and N. P. Ong, Orthogonal magnetization and symmetry breaking in pyrochlore iridate Eu$_2$Ir$_2$O$_7$, Nat. Phys. **13**, 599 (2017).

[53] J. M. Murray, O. Vafek, and L. Balents, Incommensurate spin density wave at a ferromagnetic quantum critical point in a three-dimensional parabolic semimetal, Phys. Rev. B **92**, 035137 (2015).

[54] P. Goswami, B. Roy, and S. Das Sarma, Competing orders and topology in the global phase diagram of pyrochlore iridates, Phys. Rev. B **95**, 085120 (2017).

[55] I. Boettcher and I. F. Herbut, Anisotropy induces non-Fermi-liquid behavior and nematic magnetic order in three-dimensional Luttinger semimetals, Phys. Rev. B **95**, 075149 (2017).

[56] B. Cheng, T. Ohtsuki, D. Chaudhuri, S. Nakatsuji, M. Lippmaa, and N. P. Armitage, Dielectric anomalies and interactions in the three-dimensional quadratic band touching Luttinger semimetal Pr$_2$Ir$_2$O$_7$, Nat. Commun. **8**, 2097 (2017).

[57] X.-P. Yao and G. Chen, Pr$_2$Ir$_2$O$_7$: When Luttinger Semimetal Meets Melko-Hertog-Gingras Spin Ice State, Phys. Rev. X **8**, 041039 (2018).

[58] H. Isobe and L. Fu, Quantum critical points of $j = \frac{3}{2}$ Dirac electrons in antiperovskite topological crystalline insulators, Phys. Rev. B **93**, 241113(R) (2016).

[59] B. Roy, M. P. Kennett, K. Yang, and V. Juričić, From Birefringent Electrons to a Marginal or Non-Fermi Liquid of Relativistic Spin-1/2 Fermions: An Emergent Superuniversality, Phys. Rev. Lett. **121**, 157602 (2018).

[60] I. F. Herbut, I. Boettcher, and S. Mandal, Ground state of the three-dimensional BCS *d*-wave superconductor, Phys. Rev. B **100**, 104503 (2019).

[61] N. D. Mermin, *d*-wave pairing near the transition temperature, Phys. Rev. A **9**, 868 (1974).

[62] M. Alidoust, M. Willatzen, and A-P. Jauho, Control of superconducting pairing symmetries in monolayer black phosphorus, Phys. Rev. B **99**, 125417 (2019).

[63] M. Alidoust and K. Halterman, Evolution of pair correlation symmetries and supercurrent reversal in tilted Weyl semimetals, Phys. Rev. B **101**, 035120 (2020).

[64] A. Sirohi, S. Das, P. Adhikary, R. Roy Chowdhury, A. Vashist, Y. Singh, S. Gayen, T. Das, and G. Sheet, Mixed type I and type

II superconductivity due to intrinsic electronic inhomogeneities in the type II Dirac semimetal PdTe$_2$, J. Phys. Condens. Matter **31**, 085701 (2019).

[65] I. Boettcher, Optical response of Luttinger semimetals in the normal and superconducting states, Phys. Rev. B **99**, 125146 (2019).

[66] S. Tchoumakov and W. Witczak-Krempa, Dielectric and electronic properties of three-dimensional Luttinger semimetals with a quadratic band touching, Phys. Rev. B **100**, 075104 (2019).

[67] I. Mandal, Search for plasmons in isotropic Luttinger semimetals, Ann. Phys. **406**, 173 (2019).

[68] A. Mauri and M. Polini, Dielectric function and plasmons of doped three-dimensional Luttinger semimetals, Phys. Rev. B **100**, 165115 (2019).

[69] S. Tchoumakov, L. J. Godbout, and W. Witczak-Krempa, Superconductivity from coulomb repulsion in three-dimensional quadratic band touching Luttinger semimetals, Phys. Rev. Res. **2**, 013230 (2020).

[70] C. Timm, A. P. Schnyder, D. F. Agterberg, and P. M. R. Brydon, Inflated nodes and surface states in superconducting half-Heusler compounds, Phys. Rev. B **96**, 094526 (2017).

[71] T. Bzdušek and M. Sigrist, Robust doubly charged nodal lines and nodal surfaces in centrosymmetric systems, Phys. Rev. B **96**, 155105 (2017).

[72] P. M. R. Brydon, D. F. Agterberg, H. Menke, and C. Timm, Bogoliubov Fermi surfaces: General theory, magnetic order, and topology, Phys. Rev. B **98**, 224509 (2018).

[73] H. Menke, C. Timm, and P. M. R. Brydon, Bogoliubov Fermi surfaces stabilized by spin-orbit coupling, Phys. Rev. B **100**, 224505 (2019).

[74] C. Setty, S. Bhattacharyya, Y. Cao, A. Kreisel, and P. J. Hirschfeld, Topological ultranodal pair states in iron-based superconductors, Nat. Commun. **11**, 523 (2020).

[75] C. J. Lapp, G. Börner, and C. Timm, Experimental consequences of Bogoliubov Fermi surfaces, Phys. Rev. B **101**, 024505 (2020).

[76] H. Oh and E.-G. Moon, Instability of $j = 3/2$ Bogoliubov Fermi-surfaces, arXiv:1911.08487.

[77] P. A. Frigeri, D. F. Agterberg, A. Koga, and M. Sigrist, Superconductivity without Inversion Symmetry: MnSi versus CePt$_3$Si, Phys. Rev. Lett. **92**, 097001 (2004).

[78] M. H. Fischer, M. Sigrist, and D. F. Agterberg, Superconductivity without Inversion and Time-Reversal Symmetries, Phys. Rev. Lett. **121**, 157003 (2018).

[79] T. H. Hsieh, J. Liu, and L. Fu, Topological crystalline insulators and Dirac octets in antiperovskites, Phys. Rev. B **90**, 081112(R) (2014).

[80] I. F. Herbut, Hidden role of antiunitary operators in Fierz transformation, Phys. Rev. D **100**, 116015 (2019).

[81] Y. Kawaguchi and M. Ueda, Symmetry classification of spinor Bose-Einstein condensates, Phys. Rev. A **84**, 053616 (2011).

[82] N. B. M. Schröter, S. Stolz, K. Manna, F. de Juan, M. G. Vergniory, J. A. Krieger1, D. Pei, P. Dudin, T. K. Kim, C. Cacho, B. Bradlyn, H. Borrmann, M. Schmidt, R. Widmer, V. Strokov, and C. Felser, Observation and manipulation of maximal Chern numbers in the chiral topological semimetal PdGa, arXiv:1907.08723.

[83] G. B. Sim, M. J. Park, and S. B. Lee, Triplet-superconductivity in triple-band crossings, arXiv:1909.04015.